Atmos. Chem. Phys., 26, 7463–7483, 2026
https://doi.org/10.5194/acp-26-7463-2026
© Author(s) 2026. This work is distributed under
the Creative Commons Attribution 4.0 License.

Atmospheric Chemistry and Physics
Open Access
EGU

Research article

G6-1.5K-SAI and G6sulfur: changes in impacts and uncertainty depending on stratospheric aerosol injection strategy in the Geoengineering Model Intercomparison Project

Walker Raymond Lee[1], Daniele Visioni[2], Benjamin Moore Wagman[3], Christopher Robert Wentland[3], Ben Kravitz[4,5], Shingo Watanabe[6,7], Takashi Sekiya[6], Andy Jones[8], Jim Haywood[8], Matthew Henry[8], and Ewa Monika Bednarz[9,10]

[1]Climate & Global Dynamics Division, National Science Foundation's National Center for Atmospheric Research (NSF NCAR), Boulder, CO, USA
[2]Department of Earth and Atmospheric Sciences, Cornell University, Ithaca, NY, USA
[3]Sandia National Laboratories, Albuquerque, NM, USA
[4]Department of Earth and Atmospheric Sciences, Indiana University Bloomington, Bloomington, IN, USA
[5]Atmospheric, Climate, and Earth Sciences Division, Pacific Northwest National Laboratory, Richland, WA, USA
[6]Japan Agency for Marine-Earth Science and Technology (JAMSTEC), Yokohama, Kanagawa, Japan
[7]Advanced Institute for Marine Ecosystem Change (WPI-AIMEC), Tohoku University, Sendai, Japan
[8]Department of Mathematics and Statistics, University of Exeter, Exeter, UK
[9]Cooperative Institute for Research in Environmental Sciences (CIRES), University of Colorado Boulder, Boulder, CO, USA
[10]National Oceanographic and Atmospheric Administration Chemical Sciences Laboratory (NOAA CSL), Boulder, CO, USA

Correspondence: Walker Raymond Lee (walkerl@ucar.edu)

Received: 18 November 2025 – Discussion started: 21 November 2025
Revised: 25 April 2026 – Accepted: 12 May 2026 – Published: 29 May 2026

Abstract. We report initial results for G6-1.5K-SAI, a climate model experiment proposed by the Geoengineering Model Intercomparison Project (GeoMIP). G6-1.5K-SAI simulates a stratospheric aerosol injection (SAI) to limit global warming to $\sim 1.5\,^{\circ}\mathrm{C}$ above preindustrial in each model and features several design updates relative to previous GeoMIP experiment G6sulfur, such as hemispherically symmetric subtropical injection (30° N and 30° S) instead of equatorial injection. Due to differences in climate sensitivity, models disagree on the amount of warming to be offset, and therefore on the total injection required. While they agree strongly on the rate of cooling per unit rate of injection ($\sim 0.1\,^{\circ}\mathrm{C}\,(\mathrm{Tg\,SO_2\,yr^{-1}})^{-1}$, a similar value to G6sulfur models with interactive SO_2), similarities in aerosol representation and disagreements in aerosol optical depth (AOD) per rate of unit injection and in rate of cooling per unit AOD mean this agreement may not imply accuracy. In all participating models, SAI cools the land surface more than the ocean and offsets mid- and high-latitude precipitation increases under global warming, but models disagree on the magnitude of residual Arctic amplification and changes to tropical precipitation. Relative to G6sulfur, G6-1.5K-SAI cools the Arctic more strongly, and also decreases precipitation less, especially in the tropics and over land. All in all, while the new G6-1.5K-SAI experiment constitutes an update over the older G6sulfur, due to the differences in scenario across these two experiments, any differences in SAI impacts must be evaluated carefully.

Published by Copernicus Publications on behalf of the European Geosciences Union.

1 Introduction

Solar radiation modification (SRM), also known as geoengineering, solar geoengineering, solar radiation management, climate engineering, or climate intervention, refers to a family of proposed approaches designed to cool the planet and offset some impacts of global warming by reflecting sunlight back to space (National Academies of Sciences, Engineering, and Medicine, 2021; Haywood et al., 2025; Shine et al., 2025). Stratospheric aerosol injection (SAI) – the artificial placement of aerosols or aerosol precursors into the lower stratosphere to scatter sunlight (Budyko, 1977; Crutzen, 2006) – is among the best understood modes of SRM; climate model simulations have shown that SAI would cool the planet in a global sense (e.g., Visioni et al., 2021), but continued rigorous evaluation is necessary to ensure a thorough understanding of the physical impacts of SAI, especially on a regional scale, and correctly inform policy decisions.

The Geoengineering Model Intercomparison Project (GeoMIP) was introduced by Kravitz et al. (2011) to propose standardized multi-model experiments of SRM, facilitate the comparison of results, and analyze robustness across models. Since its inception, GeoMIP experiments have included solar dimming, SAI, surface albedo modification, and marine cloud brightening; the most recent Tier 1 GeoMIP experiments, G6sulfur and G6solar, were proposed in 2015 (Kravitz et al., 2015) to synchronize phase 6 of GeoMIP with phase 6 of the Climate Model Intercomparison Project (CMIP6). These experiments also integrated scenarios from ScenarioMIP by utilizing the Tier 1 high- and medium-forcing scenarios (O'Neill et al., 2014), which would later be defined as SSP5-8.5 and SSP2-4.5, respectively (O'Neill et al., 2016). The G6sulfur and G6solar experiments prescribed 80-year SRM interventions in the 2020–2100 period against SSP5-8.5 emissions, with the amount of SRM being chosen to reduce global mean temperatures from SSP5-8.5 levels to SSP2-4.5 levels throughout. In the G6sulfur experiment, SAI is deployed near the equator, either via SO_2 injection (for models capable of simulating the evolution of aerosols) or by copying and scaling the radiative forcing fields from another model; in the G6solar experiment, the global solar constant is reduced uniformly. Preliminary results of G6sulfur and G6solar were presented by Visioni et al. (2021), who reported the mean and spread of forcing, stratospheric and surface temperature, and precipitation changes, as well as differences in aerosol behavior. The experiments have been since been used for in-depth analyses of Earth system responses to SRM, including glacier surface mass balance (Fernández et al., 2024), renewable wind energy potential (Baur et al., 2024), water deficit risk in Central Africa (Fotso-Nguemo et al., 2024), Antarctic ice shelf stability (Moore et al., 2024), and many others.

Since the initial proposal of G6sulfur in 2015, SAI design space research has evolved substantially. Kravitz et al. (2016) and MacMartin et al. (2017) identified three separate degrees of freedom by which surface temperature can be regulated by SO_2 injections at different latitudes: in addition to global mean temperature ("T_0", managed by controlling the total mass of SO_2 injected), the interhemispheric temperature gradient ("T_1") can be managed by adjusting the ratio of forcing in each hemisphere, and the equator-to-pole temperature gradient ("T_2") can be managed by adjusting the proximity of forcing to the equator or the poles. Kravitz et al. (2017) managed T_0, T_1, and T_2 in the Community Earth System Model (CESM1) by injecting SO_2 at 30° N, 15° N, 15° S, and 30° S in independent quantities, leading to the creation of the Geoengineering Large Ensemble, or GLENS (Tilmes et al., 2018). Several subsequent experiments used the same framework of the simultaneous managing of T_0, T_1, and T_2, usually with injection at the same four latitudes, including overshoot scenarios in CESM2 (Tilmes et al., 2020); exploration of different temperature targets and delayed start, phase-out, and termination scenarios (MacMartin et al., 2022); and the application of the same methodology to non-temperature-based targets (Lee et al., 2020). The similar ARISE-SAI-1.5 standardized modeling experiment was conducted in CESM2 by Richter et al. (2022) and in the UK Earth System Model (UKESM1) by Henry et al. (2023). Wells et al. (2024) also applied the same multi-objective T_0-T_1-T_2 strategy to the G6sulfur scenario in UKESM1, which they called G6controller. Conversely, comparisons of equatorial to off-equatorial injection have generally found that the former tends to over-confine aerosols to the tropical pipe, overcooling the tropics and undercooling the poles (e.g., Bednarz et al., 2023; Henry et al., 2024).

With CMIP7 approaching, the G6-1.5K-SAI experiment was proposed by GeoMIP in 2024 (Visioni et al., 2024) to serve as a successor to G6sulfur, featuring advancements in SAI design understanding, in which models can participate to bridge the gap between CMIP6 and CMIP7. The proposal aimed to design a policy- and science-relevant simulation of SAI which could be conducted by both CMIP6- and CMIP7-participating models to evaluate impacts and quantify uncertainties of an SAI deployment both across models in the same generation and across models in subsequent generations. G6-1.5K-SAI revisits several design decisions relative to G6sulfur, including underlying greenhouse warming scenario, timeline (i.e. start and end dates of the deployment), objectives (targets or goals of SAI), and injection strategy (injection location, seasonality, and amount). In this study, we present results of G6-SAI-1.5K simulations from four participating Earth system models, including SO_2 injection rates needed to meet the specified temperature target, stratospheric aerosol optical depth and sulfate burden, aerosol characteristics, and surface temperature and precipi-

tation. Additionally, we put the results in a broader context by comparing selected results with certain previous SAI modeling experiments mentioned above.

2 Methods

2.1 Experiment description

For each of the four participating models, we present two sets of simulations: an ensemble modeling the SSP2-4.5 global warming scenario without SAI, and an ensemble modeling SSP2-4.5 in which SAI is used to cool the planet in accordance with the protocols of the G6-1.5K-SAI experiment (Visioni et al., 2024), described below. SSP2-4.5, part of the Shared Socioeconomic Pathway framework (O'Neill et al., 2014, 2016) used in CMIP6, is a moderate-warming, "middle-of-the-road" scenario in which GHG emission trajectories do not markedly depart from historical trends. Of the primary SSP scenarios, SSP2-4.5 most closely matches emissions pledges in the near- to medium-term future (Burgess et al., 2020). The simulations of SSP2-4.5 considered in this study begin in model year 2015, and we consider data from the beginning of model year 2015 through the end of model year 2084.

In the G6-1.5K-SAI experiment, SAI is used to offset the warming in the SSP2-4.5 scenario. This is implemented in each model by placing SO_2 into the gridboxes nearest 30° N and 30° S latitude at approximately 21 km altitude. Injection begins in model year 2035 and continues through the end of model year 2084. The amount of injected SO_2 is chosen each year to regulate global mean near-surface air temperature (GMSAT); for each model, a target GMSAT is defined, equivalent to the SSP2-4.5 ensemble mean GMSAT averaged over the 2020–2039 period (serving as a proxy for 1.5 °C above preindustrial, as in Richter et al., 2022), and in each G6-1.5K-SAI simulation, injection rates are chosen each year to offset warming above this temperature target, with the total SO_2 divided evenly between the 30° N and 30° S injection sites. The necessary injection rates are computed separately for each ensemble member. To date, all participating models use a feedback control algorithm to compute the necessary injection rates (MacMartin et al., 2017), but this is done for convenience and is not strictly necessary. A more complete discussion of the major design decisions of G6-1.5K-SAI, and the reasoning behind them, can be found in Visioni et al. (2024).

2.2 Participating models

Thus far, four ESMs have participated in the experiment: in alphabetical order, they are version 2 of the Community Earth System Model, CESM2(WACCM6) (henceforth "CESM"); version 3 of the Energy Exascale Earth System Model, E3SMv3 (henceforth "E3SM"); the Model for Interdisciplinary Research on Climate, MIROC-ES2H (henceforth "MIROC"); and version 1.1 of the UK Earth System Model, UKESM1.1 (henceforth "UKESM"). These four ESMs, their configurations, experimental ensemble sizes, and specifications for SO_2 injection are described in Table 1. Additional information about their aerosol representations is presented in Sect. 2.3.

2.3 Aerosol representation

All four participating models use modal aerosol representation, wherein aerosol populations are described by multiple "modes" with prescribed log-normal size distributions. The configurations of CESM and E3SM used in this study both use updated versions of the Modal Aerosol Module version 3 (MAM3), first presented by Liu et al. (2012); MAM3 represents sulfate aerosols using Aitken, accumulation, and coarse modes. CESM uses MAM4 (Liu et al., 2016), which uses the same three modes for sulfate as MAM3, with some subsequent modifications to size distributions described by Mills et al. (2016); the fourth mode (nucleation) is not used to represent sulfate. E3SM uses MAM5-PSA ("Prognostic stratospheric aerosol," Hu et al., 2025), which uses the same three modes for sulfate as MAM4 (with some size modifications from Mills et al., 2016) while adding an additional coarse mode specifically for stratospheric sulfate. MIROC represents aerosol chemistry using the CHASER atmospheric chemistry model, and represents aerosol transport using the SPRINTARS aerosol transport model (Sekiya et al., 2016). This configuration represents sulfate aerosols with nucleation, Aitken, and accumulation modes. Importantly, the aerosols are not fully coupled with the radiation such that during radiation calculations, all aerosols are treated as a single mode with a prescribed size distribution. UKESM uses the five-mode version of the two-moment GLOMAP aerosol scheme (Global Model of Aerosol Processes; Mulcahy et al., 2020), which represents sulfate using nucleation, soluble Aitken, accumulation, and coarse modes (the fifth mode, insoluble Aitken, does not include sulfate). Size parameters for each mode for each participating model are included in Table 2 below.

3 Results

3.1 GMSAT, injection rates, and aerosol characterization

In Fig. 1, we present the evolution of global mean near-surface air temperature (GMSAT) for participating models. The models have a range of baseline climate states (and thus temperature targets) and rates of warming; the temperature targets cover a spread of approximately 0.5 °C, and on average, the models predict 0.30 ± 0.07 °C of warming per decade in the SSP2-4.5 scenario (where $\pm$ indicates one standard deviation across the four model ensemble means; this measure of uncertainty is used henceforth). In all participating models, SAI cools the planet (1.43 ± 0.35 °C), and

https://doi.org/10.5194/acp-26-7463-2026

Table 1. Participating Earth system models. Note that different models use different documentation conventions, meaning units may differ. The following abbreviations and acronyms are used: "Atm." for "atmosphere"; "inj." for "injection"; "GMSAT" for "global mean near-surface air temperature"; "PI" for "pre-industrial". For multi-model means, the means of the four models are weighted equally, and ± denotes one standard deviation across the ensemble means of the individual models.

Model	CESM	E3SM	MIROC	UKESM	Multi-model mean
Full model name and version, with references	CESM2(WACCM6) (Danabasoglu et al., 2020)	E3SMv3 (Xie et al., 2025)	MIROC-ES2H (Kawamiya et al., 2020)	UKESM (Mulcahy et al., 2023)	
Atm. resolution (horizontal)	1.25° lon × 0.9° lat	1.0° lon × 1.0° lat (physics; 1.5° for dynamics)	1.4° lon × 1.4° lat (2.8° for chemistry)	1.875° lon × 1.25° lat	
Atm. resolution (vertical)	70 levels up to 10^{-6} hPa	80 levels up to ∼ 60 km	90 levels up to 87 km	85 levels up to 85 km	
Ensemble size	3 (G6-1.5K-SAI), 5 (SSP2-4.5)	3	10	3	
SO_2 inj. altitude	47.1–39.3 hPa (∼ 21.6 km)	21 km	21 km	21.5 km	
SO_2 inj. latitude (both hemispheres)	30.6°	29.5°	29.3°	30.6°	
PI average	287.07 K	286.73 K	287.75 K	286.97 K	287.13 ± 0.44 K
GMSAT target	288.64 K (PI + 1.6 °C)	288.44 K (PI + 1.7 °C)	288.70 K (PI + 0.9 °C)	288.92 K (PI + 2.0 °C)	288.71 ± 0.25 K (PI + 1.6 ± 0.5 °C)
SSP2-4.5 warming per decade	0.288 °C	0.307 °C	0.221 °C	0.388 °C	0.301 ± 0.069 °C
SAI cooling, 2065–2084	1.28 °C	1.49 °C	1.07 °C	1.88 °C	1.43 ± 0.35 °C
SO_2 injection rate, 2065–2084	11.69 Tg yr^{-1}	15.03 Tg yr^{-1}	8.91 Tg yr^{-1}	14.48 Tg yr^{-1}	12.53 ± 2.82 Tg yr^{-1}

Table 2. Size parameters for sulfate aerosol representation in participating models. Each model reports size distributions using different measurements, which are not easily converted into a common one; here, diameters have been converted into radii and all measurements are reported in units of µm, but parameter descriptions are otherwise preserved from their original sources, as indicated in the first row. σ_g denotes geometric standard deviation for a lognormal distribution. For CESM, data are sourced from Visioni et al. (2023, Table 1); Liu et al. (2012, Table 1); and Mills et al. (2016, Appendix B). For E3SM, data are sourced from Hu et al. (2025, Sect. 2.1 and Fig. 1a); Liu et al. (2012, Table 1); and Mills et al. (2016, Appendix B). For MIROC, data are sourced from Sekiya et al. (2016, Table 2 and Sect. 2.1). For UKESM, data are sourced from Mulcahy et al. (2020, Table 1).

Mode	CESM (r = dry radius)	E3SM (r = geometric median dry radius)	MIROC (r = dry radius; μ_r = mean radius)	UKESM (r = geometric mean dry radius)
Nucleation			$\sigma_g = 1.6$ $0.0005 < r < 0.005\,\mu m$	$\sigma_g = 1.59$ $0.0005 < r < 0.005\,\mu m$
Aitken	$\sigma_g = 1.6$ $0.030 < r < 0.106\,\mu m$	$\sigma_g = 1.6$ $0.030 < r < 0.106\,\mu m$	$\sigma_g = 1.6$ $0.005 < r < 0.05\,\mu m$	$\sigma_g = 1.59$ $0.005 < r < 0.05\,\mu m$
Accumulation	$\sigma_g = 1.6$ $0.116 < r < 0.96\,\mu m$	$\sigma_g = 1.6$ $0.1070 < r < 0.96\,\mu m$	$\sigma_g = 1.2$ $0.05\,\mu m < r$	$\sigma_g = 1.40$ $0.05 < r < 0.25\,\mu m$
Coarse	$\sigma_g = 1.2$ $0.8 < r < 80\,\mu m$	$\sigma_g = 1.8$ $0.8 < r < 80\,\mu m$		$\sigma_g = 2.00$ $0.25 < r < 5\,\mu m$
Stratospheric coarse		$\sigma_g = 1.2$ $0.8 < r < 80\,\mu m$		
Radiation scheme			$\sigma_g = 2.0$ $\mu_r = 0.243\,\mu m$	

the chosen injection rates reduce GMSAT to approximately maintain the temperature target. In any given year, there is a non-zero amount of error, or difference between each model's temperature target and the actual GMSAT; the difference across models in which the injections are able to maintain the temperature targets is a function not only of natural variability and aerosol behavior in each model, but also of the tuning of the controller used to choose injection rates. Diagnostics of this error are presented in Sect. S1 of the Supplementary Material. For the purposes of this study, any analysis which considers the amount of cooling (e.g., cooling per unit AOD in Fig. 2e, maps of cooling in Figs. 5–6) will consider the amount of actual cooling effected by the intervention in each model (i.e., SSP2-4.5 temperature minus G6-1.5K-SAI temperature) and not the intended cooling (i.e., SSP2-4.5 temperature minus the temperature target).

Figure 2 denotes the magnitude of the intervention required to offset warming above the GMSAT target in each model. Averaged over the last two decades of the experimental period (2065–2084), the models require $12.53 \pm 2.82\,Tg\,SO_2$ injection per year, producing 0.15 ± 0.06 stratospheric 550 nm aerosol optical depth (henceforth "AOD"), to cool the planet by the desired margin. The amount of SO_2 needed to cool the planet in each model is a function of both the amount of warming to be offset and how effectively aerosols cools the surface; the latter is governed by the models' respective aerosol microphysics, chemistry and transport representations (which determine the timescale for SO_2 oxidation, aerosol transport, particle growth, absorption and scattering of visible and infrared radiation, and particle lifetime) and internal climate feedbacks.

While there is considerable uncertainty in the required total injection rates and AOD across models (Fig. 2a–b), the models strongly agree on the overall ratio of cooling per unit injection (Fig. 2c; $0.11 \pm 0.01\,°C\,(Tg\,SO_2\,yr^{-1})^{-1}$). This is within the commonly-cited 8–16 $Tg\,SO_2\,yr^{-1}\,°C^{-1}$ range for SAI (Haywood et al., 2022, 2025); however, given the disagreement in AOD per unit injection (2d) and cooling per unit AOD (2e), and that the models use similar aerosol representation and are trained on the same volcanic eruptions, the agreement seen in 2c may not imply accuracy. Of the four participating models, CESM and UKESM show higher AOD per unit injection (2d) but lower cooling per unit AOD (2e), while E3SM and MIROC show the reverse. As a whole, Fig. 2c suggests higher cooling per unit injection and tighter model agreement for G6-1.5K-SAI than for G6sulfur; however, this is mainly because of the lower cooling per unit injection in the MPI models in G6sulfur, which disagree with the other three. The four G6-1.5K-SAI models cool the planet at similar rates per unit injection to the three G6sulfur models with interactive SO_2 injection, but as these models also include CESM2 and an earlier version of UKESM which also used GLOMAP, this agreement again may not imply accuracy. We elaborate more on this in Sect. 4.

The three interactive-SO_2 G6sulfur models produced, as a whole, similar or more AOD per unit injection than G6-1.5K-SAI models (2d). The literature disagrees on whether subtropical injection would produce AOD more or less efficiently than equatorial injection; due to the poleward direc-

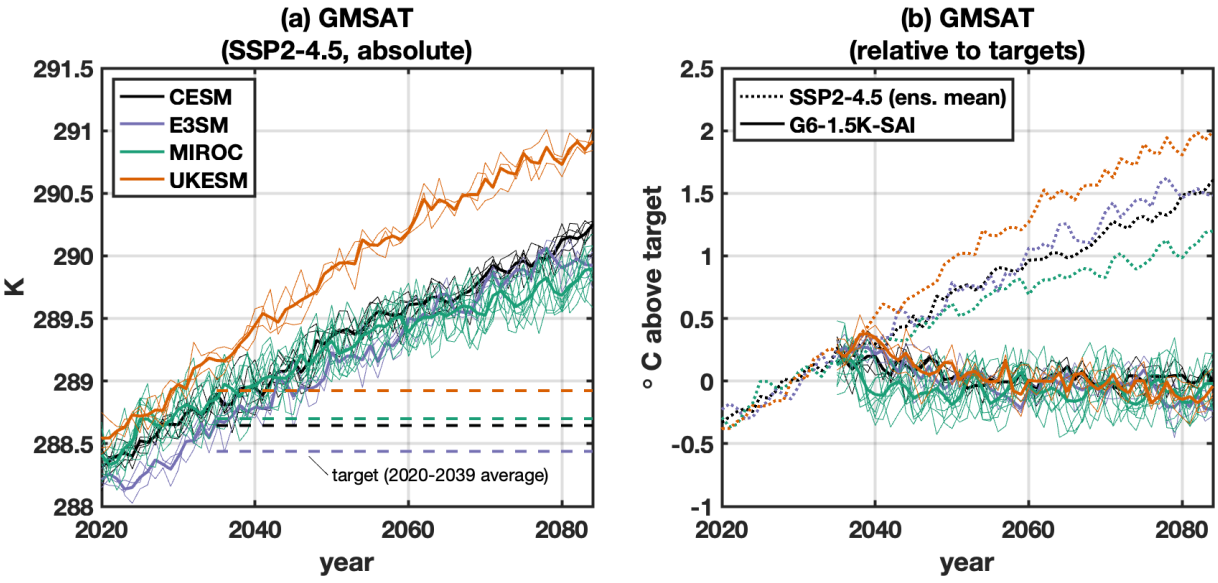

Figure 1. Global mean near-surface air temperature (GMSAT) for participating models. Panel **(a)** plots absolute GMSAT for the SSP2-4.5 scenario; dashed lines indicate each model's temperature target, defined as the 2020–2039 ensemble mean. Panel **(b)** plots GMSAT relative to each model's respective target; dotted lines show SSP2-4.5 ensemble means, and solid lines show G6-1.5K-SAI data. In both panels, thin lines show individual ensemble members, and bolded lines show ensemble means.

tion of the stratospheric Brewer-Dobson circulation, stratospheric aerosols tend to be carried towards the higher latiutdes, however, the lifetime of aerosols decreases as aerosols are injected away from the tropical pipe and into the subtropics. Visioni et al. (2023) report more AOD for prescribed equatorial injection in a multi-model comparison, but Zhang et al. (2024) report higher AOD for 30° N + 30° S injection than for equatorial when used to cool the planet in CESM2.

In a longer-term injection scenario, larger concentrations of aerosols (such as due to aerosols being confined to the tropical pipe, as is common for equatorial injections) lead to increased particle size due to coagulation, decreasing particle scattering efficacy and lifetime (e.g., Dykema et al., 2016; Kleinschmitt et al., 2018), suggesting lower AOD per unit injection for equatorial injection as rates of injection increase. Earlier modeling studies (e.g., Niemeier and Timmreck, 2015; Niemeier and Tilmes, 2017) have found that injection efficiency begins to fall off with increasing injection rates beginning at 10–20 Tg SO_2 yr^{-1}; however, for G6sulfur, the downward trend of AOD production per unit injection with time suggests such a nonlinearity even at lower injection rates in the case of equatorial injection, and this trend is absent in G6-1.5K-SAI models except CESM, suggesting such nonlinearities are smaller or absent in this regime of injection rates in these models for subtropical injection. Cooling per unit AOD (2e) follows a similar trend for the two experiments, with a larger model spread for G6-1.5K-SAI than G6sulfur.

Figure 3 plots zonal mean AOD for G6-1.5K-SAI and G6sulfur. In all G6-1.5K-SAI participating models, AOD distribution shares the same broad characteristics, consistent with the poleward direction of the stratospheric Brewer-Dobson Circulation and the transport barriers of the stratospheric polar vortices: AOD increases poleward of the injection sites, peaks near the boundary of the polar vortex, and then plateaus (Northern Hemisphere) or drops (Southern Hemisphere) near the pole. AOD is lower than the global mean equatorward of the injection sites, with the lowest point being at the equator in all models except MIROC, in which the local minimum is closer to 10° N. Models disagree on the ratio of polar AOD to tropical AOD, ranging from about 1.5 (MIROC) to about 3.5 (E3SM). The G6sulfur models have a higher AOD in the tropics, as well as a much higher uncertainty of tropical AOD; the four G6-1.5K-SAI models generally agree more strongly with each other on the shape of the AOD distribution than the G6sulfur models, even if one or both of the models that used different methods to compute AOD are excluded.

In Fig. 4, we present atmospheric sulfur lifetime and dry effective aerosol radius (R_{eff}) for participating models. Sulfur lifetime can be computed as the ratio of the global burden to the global sink, which we estimate by assuming a quasi-steady state where the sink is approximately equal to the dominant source, a method used in previous studies of stratospheric aerosol injection (e.g., Visioni et al., 2018, 2023; Henry et al., 2024). Therefore, we compute sulfur lifetime by taking the ratio of change in global sulfur burden to sulfur injection rate (the S fraction of SO_2 injection rate; note that injection rates in Fig. 4a are approximately half those in Fig. 2a). Global sulfur burden is de-

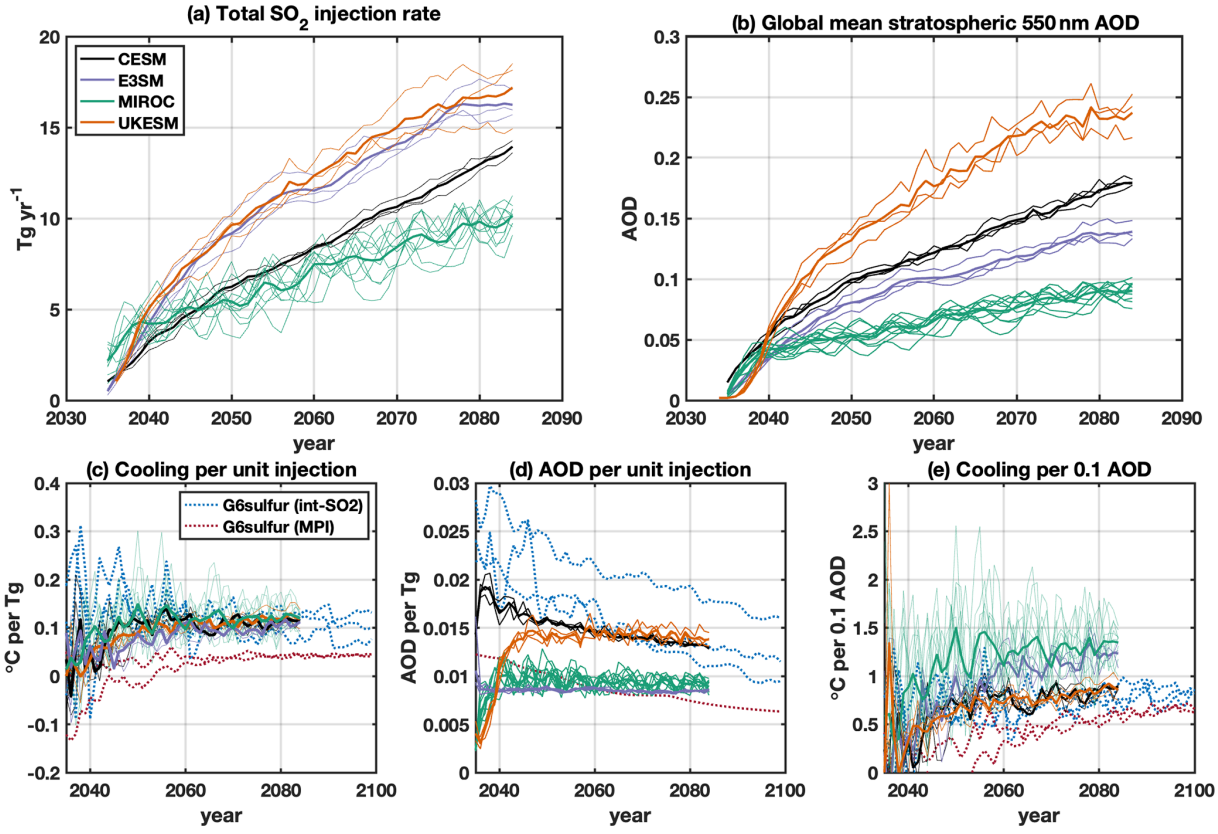

Figure 2. Interventions needed to meet the temperature target in each model, along with ratios of selected quantities and comparisons to the G6sulfur experiment. Panel **(a)** plots SO_2 annual injection rates in Tg for each year of the G6-1.5K-SAI experiment. Panel **(b)** plots global mean stratospheric 550 nm aerosol optical depth (AOD) for G6-1.5K-SAI. Panel **(c)** plots cooling (change in GMSAT) per Tg of SO_2 injected each year, panel **(d)** plots global mean 550 nm AOD per Tg of SO_2 injected each year, and panel **(e)** plots cooling (change in GMSAT) per 0.1 global mean 550 nm AOD. In all panels, thin lines denote individual ensemble members, and thick lines denote ensemble means. Panels **(c)**–**(e)** compare G6-1.5K-SAI data against the G6sulfur experiment: dotted lines represent ensemble means of G6sulfur models, with blue used for models with interactive SO_2 (CESM2-WACCM, IPSL-CM6A, and UKESM1) and red for MPI-LR and MPI-HR, which converted SO_2 injection rates into AOD offline and then prescribed the AOD into the coupled model. CNRM, which prescribed a scaled AOD distribution provided by GeoMIP, is not included in this figure.

rived from the sulfur fractions of global SO_4 burden (CESM, E3SM), global H_2SO_4 burden (UKESM), or global aerosol burden (MIROC), assuming that differences between SSP2-4.5 and G6-1.5K-SAI are dominated by the SO_2 injections. Using this method, we report sulfur lifetimes between 1 and 1.5 years for CESM, E3SM, and MIROC, and a lifetime of approximately 8 months for UKESM (Fig. 4b). Visioni et al. (2023) reported similar stratospheric sulfate lifetimes for single-latitude 30° N and 30° S injection in CESM2 and UKESM1, and Henry et al. (2024) also estimated an aerosol lifetime of less than one year for 30° N + 30° S injection in UKESM1. For comparison, Lee et al. (2023) reported lifetimes of about 16 months and 10 months for 23–25 and 19–20 km altitude SAI, respectively, in CESM1, and Visioni et al. (2018) reported lifetimes of ∼ 12–13 months for SAI in a previous generation of models.

Estimates of dry effective aerosol radius, R_{eff}, are computed using the methodology outlined by Visioni et al. (2023), Brown et al. (2024, Appendix A), and Grainger (2025); we describe this process, and the relevant equations, in Sect. S2 of the Supplementary Material. Using this method, we compute zonal mean R_{eff} averaged over 2065–2084 (using monthly output; assuming a relatively even longitudinal distribution of aerosols after 30 years of injection, we do not weight longitudinally by, for example, surface area density or mass) for G6-1.5K-SAI for participating models (Fig. 4c–f). R_{eff} peaks in the lower stratosphere for all models, with some models (E3SM and MIROC) showing a higher variance in latitudinal size distribution. Models report a peak Reff ranging from 0.3–0.35 µm (UKESM) to 0.4–0.45 µm (CESM). CESM has the largest R_{eff} (Visioni et al., 2023 also reported CESM2 having larger R_{eff} than the other two other participating models in that study with sectional aerosol representation); CESM has injection rates which are closest to the median of the four participating models, but also has a higher aerosol lifetime than the models which inject more.

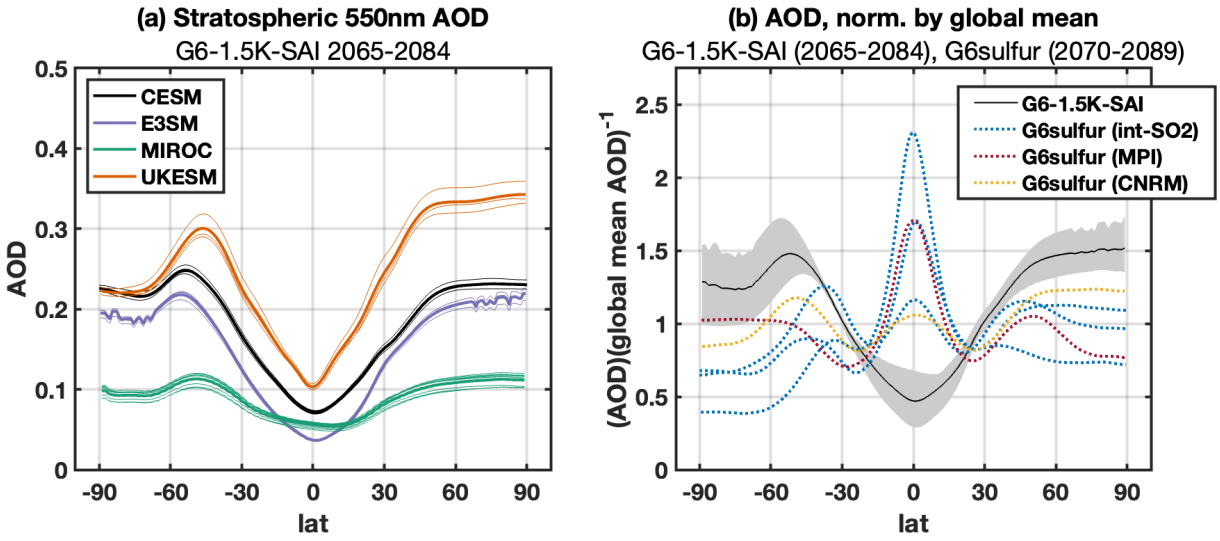

Figure 3. Latitudinal distribution of stratospheric 550 nm aerosol optical depth. Panel **(a)** plots absolute zonal mean AOD for G6-1.5K-SAI; thin lines denote individual ensemble members, and thick lines denote ensemble means. Panel **(b)** plots zonal mean AOD, normalized by the global mean AOD for each model, for G6-1.5K-SAI and G6sulfur. For G6-1.5K-SAI, the black line indicates the multi-model mean of the four ensemble means (weighted equally), and the shading denotes the spread across models. Dotted lines denote ensemble means for individual G6sulfur models, with blue for the models with interactive SO_2 injection; red for MPI-LR and MPI-HR, which converted SO_2 injection rates into AOD offline and then prescribed the AOD into the coupled model; and yellow for CNRM, which prescribed a scaled AOD distribution provided by GeoMIP. Data are averaged over 2065–2084 for G6-1.5K-SAI (in both panels) and over 2070–2089 for G6sulfur (when the G6sulfur models average approximately 1.4 °C of cooling, a similar amount to the last 20 years of G6-1.5K-SAI). For E3SM, AOD data is polar day-only, meaning that data from grid cells at high latitudes during polar winter are excluded from calculation.

UKESM, which has the smallest peak R_{eff}, has the highest injection rates but also a much shorter lifetime than the other models. As aerosols grow beyond the optimal radius for scattering sunlight for a given wavelength (Dykema et al., 2016, estimate the optimal wet radius for sulfate to be 0.30 µm), they will reflect sunlight less efficiently and cool the planet less efficiently; larger aerosols will, in general, also sediment out faster. CESM, which has the largest peak R_{eff}, is the only G6-1.5K-SAI model to show a prominent decrease of AOD per unit injection with time, as discussed above (Fig. 2d). Note that for MIROC, which assumes a single-mode size distribution for radiative calculations, the actual aerosol size distribution affects transport but not radiative transfer. For comparison, online-calculated wet effective aerosol radius is only available as model output for CESM and MIROC, and is included in the Supplementary Material (Sect. S2).

3.2 Surface temperature and precipitation response

In Figs. 5 and 6, we present maps of near-surface air temperature changes for SSP2-4.5 and G6-1.5K-SAI. Under SSP2-4.5, global warming (left column) increases surface temperatures nearly everywhere in all models, with the exceptions being the Labrador Sea in CESM and MIROC (indicative of a slowing down of the Atlantic Meridional Overturning Circulation, or AMOC, e.g., Bednarz et al., 2025); and parts of the Southern Ocean in MIROC. Arctic amplification (stronger warming in the Arctic relative to the rest of the world), a robust feature across observations and model simulations of warming (Taylor et al., 2022), is observed in all four models, and Antarctic amplification is observed in CESM, E3SM, and UKESM in SSP2-4.5. Outside of the Arctic, warming over land tends to be higher than warming over the ocean in all four models.

In all four models, G6-1.5K-SAI cools the planet everywhere or nearly everywhere (middle column). Cooling tends to be strongest at the poles, but there is still statistically significant cooling in the tropics despite the AOD minimums at or near the equator. Cooling is stronger over land than over the ocean; this has been attributed to the smaller heat capacity of air compared to water in SAI simulations (Duan et al., 2019), but could also represent the preventing of increased warming over land under global warming, which is a robust result in model simulations and has been attributed to a number of hydrological and lapse rate feedbacks (Sutton et al., 2007; Joshi et al., 2008).

The only location where G6-1.5K-SAI induces warming is parts of the Southern Ocean in MIROC; however, these are the same locations as where global warming cools the surface in the same model, meaning the temperature changes are likely indicative of circulation changes under global warming which are mitigated by the intervention.

Because SAI cools the planet by a different mechanism (reflected solar radiation) than that by which climate change

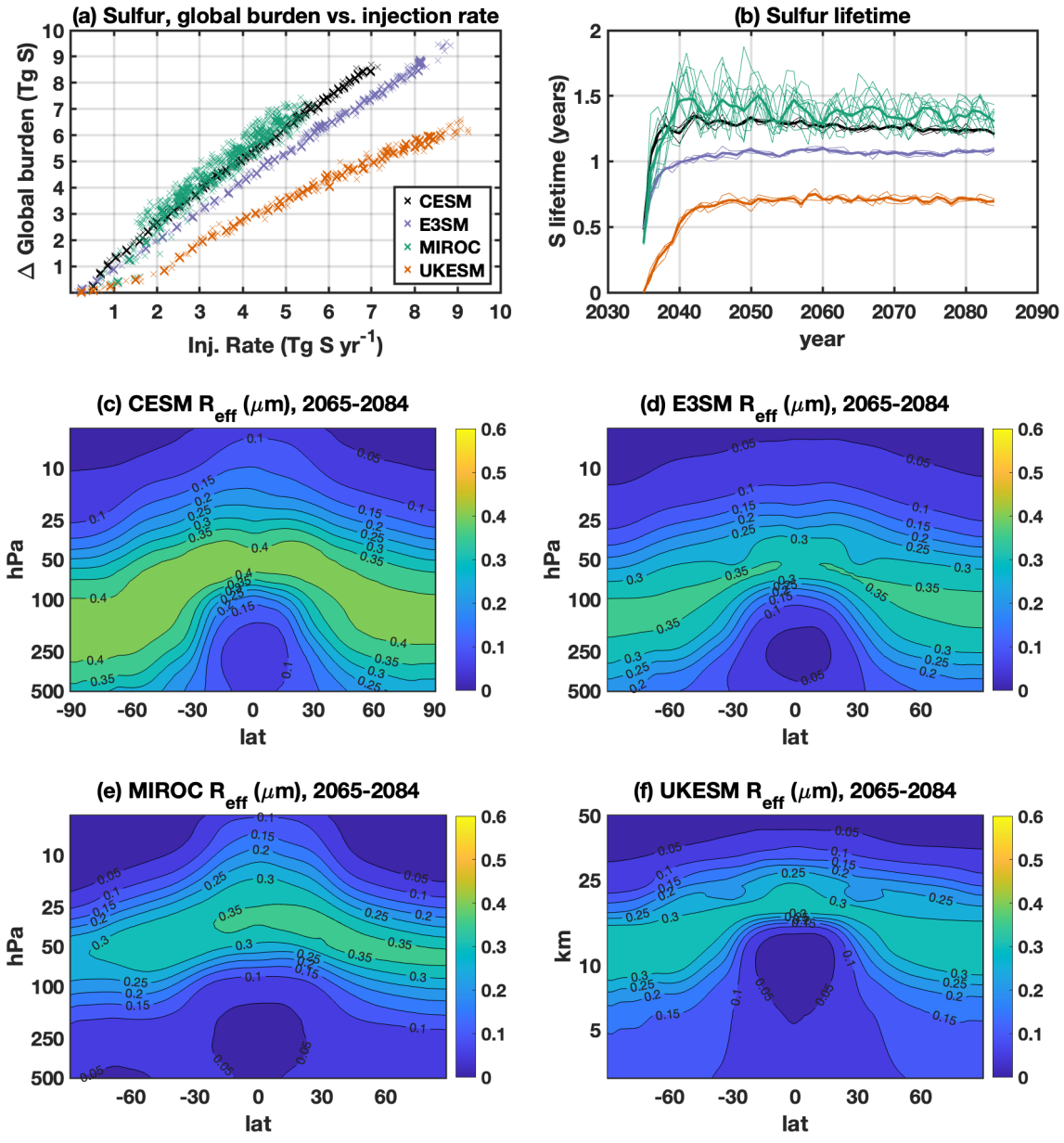

Figure 4. Sulfur lifetime and dry effective aerosol radius (R_{eff}) for G6-1.5K-SAI. Panel **(a)** plots change in global atmospheric sulfur burden (G6-1.5K-SAI minus SSP2-4.5) against SAI injection rates (in S, not SO_2) for each year of the experiment, the ratio of which is an estimate of atmospheric sulfur lifetime, shown in panel **(b)**. Thin x's **(a)** and lines **(b)** denote data from individual ensemble members; bold x's and lines denote data from ensemble means. Panels **(c)**–**(f)** plot unweighted zonal mean estimated R_{eff}, computed using the method outlined in the text, for G6-1.5K-SAI; data are averaged over the last 20 years of the experiment (2065–2084).

warms it (trapped infrared radiation), SAI does not revert a warmed climate to its pre-warmed condition; rather, the combination of greenhouse gas effect and SAI creates a new, unique climate state. The right column of Fig. 5 compares this new state with the "reference period" of SSP2-4.5 from which GMSAT targets were derived. In all four models, under SSP2-4.5, the NH warms more than the SH due to a combination of Arctic amplification and increased warming over land relative to the ocean; G6-1.5K-SAI offsets both of these mechanisms by cooling the Arctic and land surface most strongly, but the extent to which hemispherically symmetric injection at 30° latitude over- or under-compensates for each is model-dependent. By design, the reference period and the last 20 years of G6-1.5K-SAI have the same global average temperature, and so any overcooling (blue) in one part of the world must be balanced by residual warming or undercooling (red) in another. In MIROC and UKESM, most of the tropics and midlatitudes are overcooled by < 1 °C, with residual

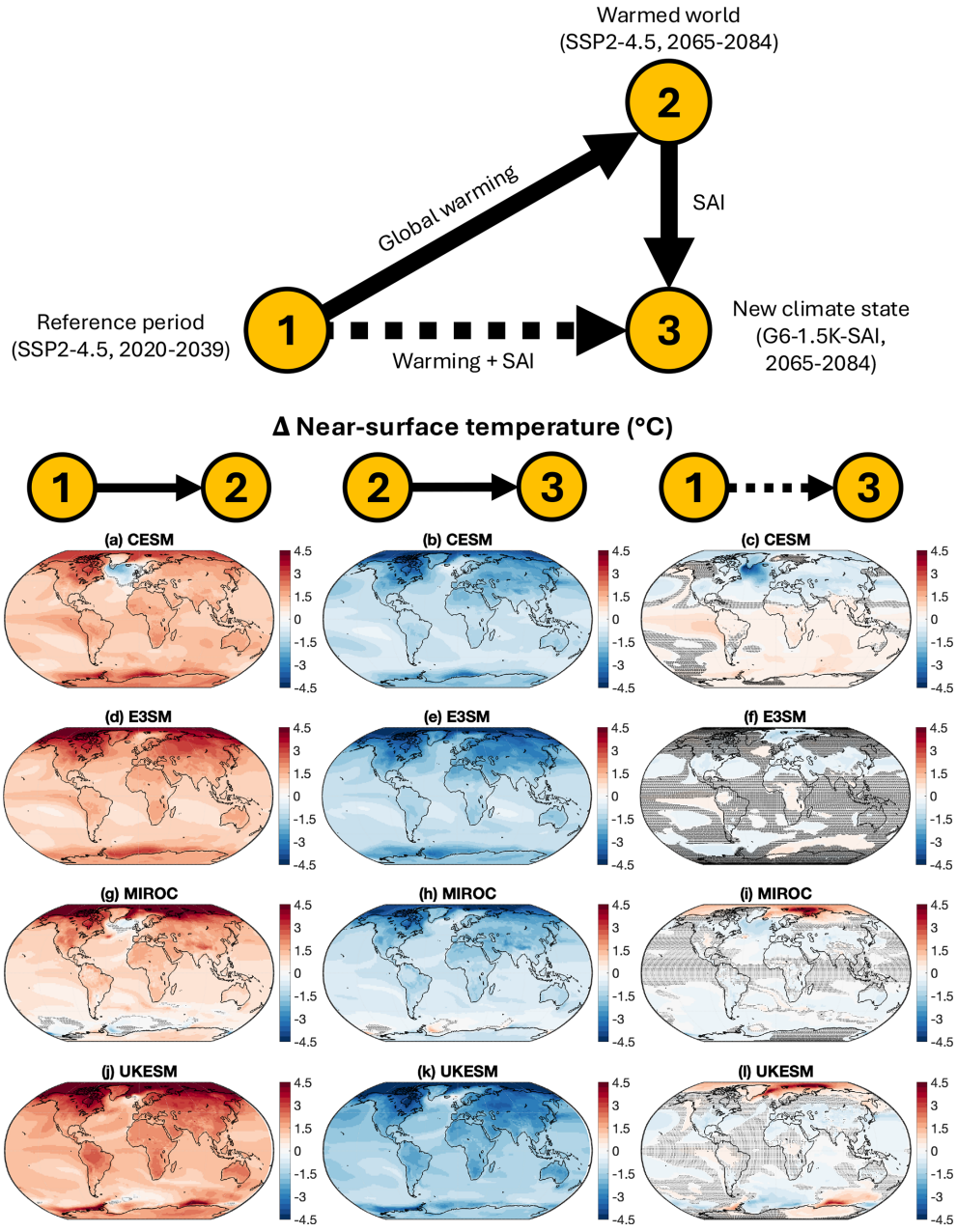

Figure 5. Maps of near-surface air temperature changes (in °C) between three different periods: (1) the reference period, 2020–2039 of SSP2-4.5, corresponding to the period over which the GMSAT targets are defined; (2) the warmed world, 2065-2084 of SSP2-4.5, corresponding to the last 20 years of the experimental period; and (3) the new climate state reached under G6-1.5K-SAI in 2065–2084. The left column plots the difference between (1) and (2), representing the changes due to global warming; the middle column plots the difference between (2) and (3), representing the changes due to G6-1.5K-SAI; and the right column plots the difference between (1) and (3), representing the combined impacts of warming and G6-1.5K-SAI. Shading represents regions with no statistically significant differences at $p = 0.05$; p values are computed for each grid cell, with samples consisting of all individual annual mean data points across all ensemble members from the respective time periods, with samples compared using the two-sample t-test.

warming at one or both poles. CESM overcools most of the Northern Hemisphere while undercooling most of the Southern Hemisphere. E3SM has the smallest temperature differences between these two periods, with no statistically significant difference across the highest portion of the planet out of the four models.

The G6-1.5K-SAI results for CESM2 and UKESM1.1 are consistent with those of several previous SAI simulations in CESM2 and UKESM1, respectively. Under the ARISE-SAI-

1.5 protocol, which manages for the same GMSAT (T_0) in the same scenario while also managing the interhemispheric (T_1) and equator-to-pole (T_2) temperature gradients, CESM2 restores reference-period surface temperatures nearly everywhere by injecting mostly ($\sim 60\,\%$) at 15° S, with additional injection ($\sim 20\,\%$ each) at 15° N and 30° S (Richter et al., 2022). This implies that equal injections in both hemispheres would overcool the NH, consistent with G6-1.5K-SAI; additionally, G6sulfur (equatorial injection) in CESM2 overcools the NH and undercools the SH, with little residual Arctic warming (Visioni et al., 2021). In UKESM1, residual temperature patterns under ARISE-SAI-1.5 (mostly 30° N and 30° S injection, but with increasing 15° N injection the last 15 years) are very similar to UKESM1.1 under G6-1.5K-SAI (Henry et al., 2023). G6controller, which aims to reduce T_0, T_1, and T_2 in the SSP5-8.5 scenario to SSP2-4.5 levels, also bears some similarities; the controller converges to mostly ($> 80\,\%$) injection at 30° N and 30° S, with significant residual Arctic amplification (Wells et al., 2024).

Figure 6 presents a comparison of the G6-1.5K-SAI and G6sulfur multi-model means. Unlike G6-1.5K-SAI, which uses a single warming scenario (SSP2-4.5) and cools the planet to maintain a fixed temperature, G6sulfur cools the planet to reduce temperatures from a high-warming scenario (SSP5-8.5) to match those of a moderate-warming scenario (SSP2-4.5). For a comparison period, we choose 2070–2089 for G6sulfur, in which the models average approximately 1.4 °C of cooling, the same as the G6-1.5K-SAI models in 2065–2084; therefore, the analogous "reference period" (period #1 in Fig. 6) with the same global mean temperature as the intervention is SSP2-4.5 2070–2089, the analogous "warmed world" with 1.4 °C of warming relative to the reference period (period #2) is SSP5-8.5 2070–2089, and the analogous "new climate state" with 1.4 °C of warming and 1.4 °C of cooling (period #3) is G6sulfur 2070–2089.

Comparing the patterns of warming in the two scenarios (left column), the G6-1.5K-SAI warming scenario (SSP2-4.5 relative to baseline) has more warming in the Arctic, while the G6sulfur warming scenario (SSP5-8.5 relative to SSP2-4.5) has more warming over land outside of the Arctic. Both scenarios have increased warming over land relative to the oceans, and more warming in the Arctic than the Antarctic. Both interventions (middle column) cool the land more than the ocean, and cool the NH more than the SH; G6-1.5K-SAI cools the Arctic and land in the NH more strongly than G6sulfur, and G6sulfur cools land in the SH more strongly than G6-1.5K-SAI. Both strategies cool Antarctica comparably to each other. Relative to their respective warming scenarios, G6sulfur has higher residual Arctic and NH midlatitude warming, and more G6sulfur models agree on where there is residual polar warming in both hemispheres (right column). Note that the residuals are functions of both the injection strategy and the scenario in which it is used; for example, G6-1.5K-SAI has more residual cooling over land in the NH, and while G6-1.5K-SAI does cool the NH land more strongly than G6sulfur, there is also less warming over land to offset in the former's warming scenario than the latter's.

In the G6-1.5K-SAI warming scenario (SSP2-4.5), there is a pattern of increased warming in the eastern tropical pacific, indicative of a positive ENSO (El Niño Southern Oscillation) response. This pattern is absent in the G6sulfur warming scenario (SSP5-8.5 minus SSP2-4.5). Under G6-1.5K-SAI, there is a cooling pattern in this region, but smaller in magnitude and size than the warming, leaving a pattern of warming in the residual. There has been some investigation as to whether and how SAI could affect ENSO; Gabriel and Robock (2015) analyzed the GeoMIP G1, G2, G3, and G4 simulations and found little change to ENSO frequency or amplitude under SRM. A study of global teleconnection patterns in CESM found little change in ENSO behavior under RCP8.5 or GLENS in CESM1, but modest changes under SSP5-8.5 in CESM2 which were offset by SAI (Rezaei et al., 2023), and another study found that under ARISE-SAI-1.5, some seasonal predictability is maintained relative to SSP2-4.5 in regions affected by ENSO teleconnections (Mayer et al., 2024). It is plausible that, in this case, the temperature patterns visible in Fig. 6 reflect modulation of ENSO (or lack thereof) under SAI; however, we leave in-depth investigation of ENSO behavior to a future study.

In Fig. 7, we present maps of precipitation changes between the same time periods as above. Under global warming, precipitation is expected to increase as the warmer atmosphere's capacity to hold water increases in accordance with the Clausius-Clayperon relation. Under SSP2-4.5 (left column), changes in all four models share common characteristics: precipitation increases in the mid- and high latitudes in both hemispheres, statistically insignificant changes in much of the subtropics and extratropics, and the largest changes near the equator, especially in the Pacific. The tropical changes generally reflect meridional shifts of precipitation, although the models disagree on the direction of the change; CESM shows a southward shift, E3SM shows a northward shift, MIROC shows a convergence at the equator from both directions, and UKESM shows only an increase without a decrease of comparable size nearby.

The impacts of G6-1.5K-SAI (middle column) are also most prominent in the tropics, midlatitudes, and poles, with all four models having the most area without any statistically significant change in the subtropics and extratropics. Cooling the planet reduces precipitation in the mid- and high latitudes in both hemispheres in all four models, offsetting the warming-induced increases. In all four models, these decreases under G6-1.5K-SAI are of comparable magnitude to the increases under SSP2-4.5. As a result, differences in the residual (right column) are statistically insignificant over large portions of the Earth's surface outside of the tropics in all four models. As with SSP2-4.5, the largest precipitation changes under G6-1.5K-SAI are found near the equator, but they are harder to characterize; some changes due

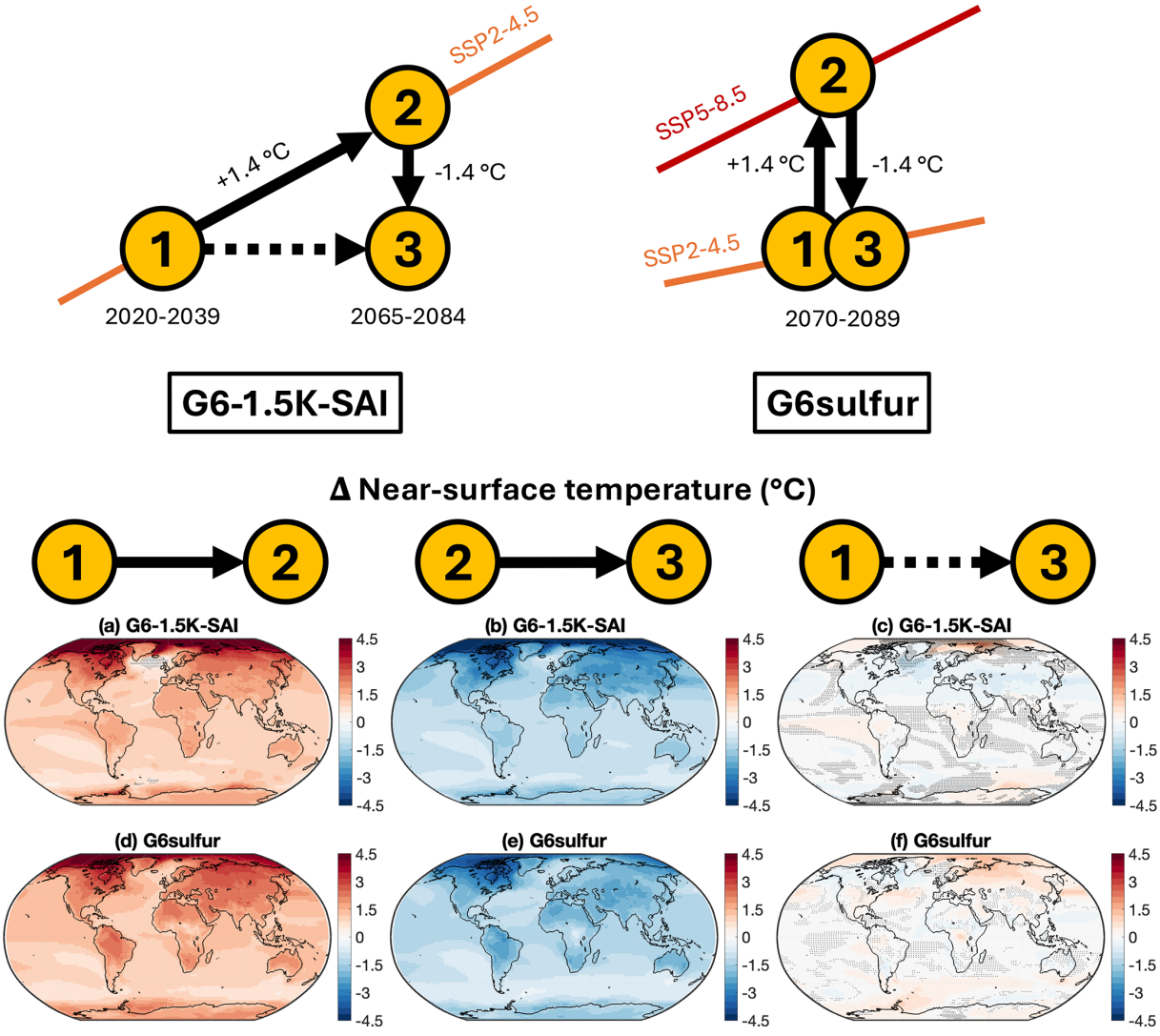

Figure 6. Maps of changes in near-surface air temperature (in °C) as in Fig. 5, for G6-1.5K-SAI and G6sulfur multi-model means (models weighted equally for both experiments). For G6sulfur, all three periods are averages of 2070–2089 data, in which the amount of cooling is approximately the same (1.4 °C) as the last 20 years of G6-1.5K-SAI: period 1 is SSP2-4.5, period 2 is SSP5-8.5, and period 3 is G6sulfur. All six G6sulfur-participating models are included (CESM2-WACCM, IPSL-CM6A, UKESM1, MPI-LR, MPI-HR, and CNRM). Shading represents areas where models disagree on the sign of the change (fewer than 3 out of 4 for G6-1.5K-SAI, and fewer than 4 out of 6 for G6sulfur).

to global warming are mitigated, others are exacerbated, and sometimes new changes are introduced.

Precipitation changes in CESM2 under G6-1.5K-SAI follow a similar pattern to those under ARISE-SAI-1.5 (see Richter et al., 2022, Fig. 6), with comparable midlatitude decreases offsetting the increases under SSP2-4.5 and a similarly-structured shift in the tropical Pacific, and precipitation responses in UKESM1.1 under G6-1.5K-SAI are generally more similar to UKESM1 G6controller than to UKESM1 G6sulfur (see Wells et al., 2024, Fig. 5). However, differences in residuals in all cases are likely functions of both differences in scenario and time period, as well as differences in strategy (see G6-1.5K-SAI and G6sulfur comparison below).

Figure 8 presents a multi-model comparison of G6-1.5K-SAI and G6sulfur, averaging over the same time periods as in Fig. 6 when both experiments cool the planet by approximately 1.4 °C. As with temperature differences, residual precipitation differences relative to the reference in each experiment (right column) must take into account differences in both the warming scenario (SSP2-4.5 for G6-1.5K-SAI, and SSP5-8.5 for G6sulfur) and the impacts of the intervention itself. In the G6sulfur warming scenario, on average, precipitation changes in the tropical Pacific ocean are similar to the warming scenario of G6-1.5K-SAI, but changes

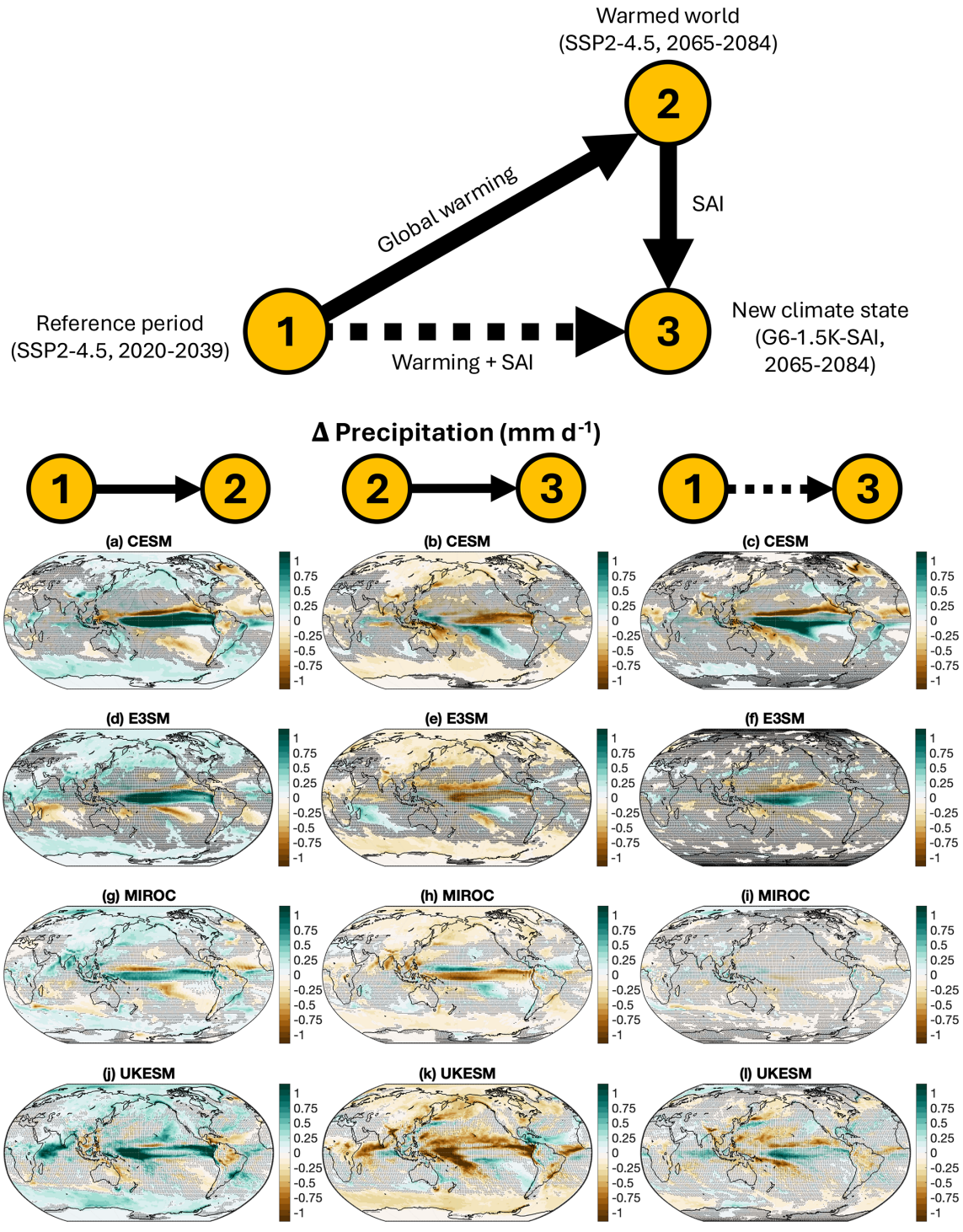

Figure 7. Maps of differences in precipitation (in mm d^{-1}) for G6-1.5K-SAI and SSP2-4.5, as in Fig. 5.

in the tropics outside of the Pacific are more pronounced. G6sulfur reduces precipitation in the tropics by a larger degree than G6-1.5K-SAI, both in the Pacific and elsewhere; G6sulfur also increases precipitation in more parts of the tropics and subtropics than G6-1.5K-SAI. Compared to the changes under their respective warming scenarios, G6-1.5K-SAI and G6sulfur both have the largest residual differences in the tropical Pacific; however, G6sulfur has a stronger net drying effect in this region, and the residual drying is also prominent over land in South America, Malaysia, and central Africa, whereas the residual precipitation differences of G6-1.5K-SAI are more concentrated in the ocean. Residual

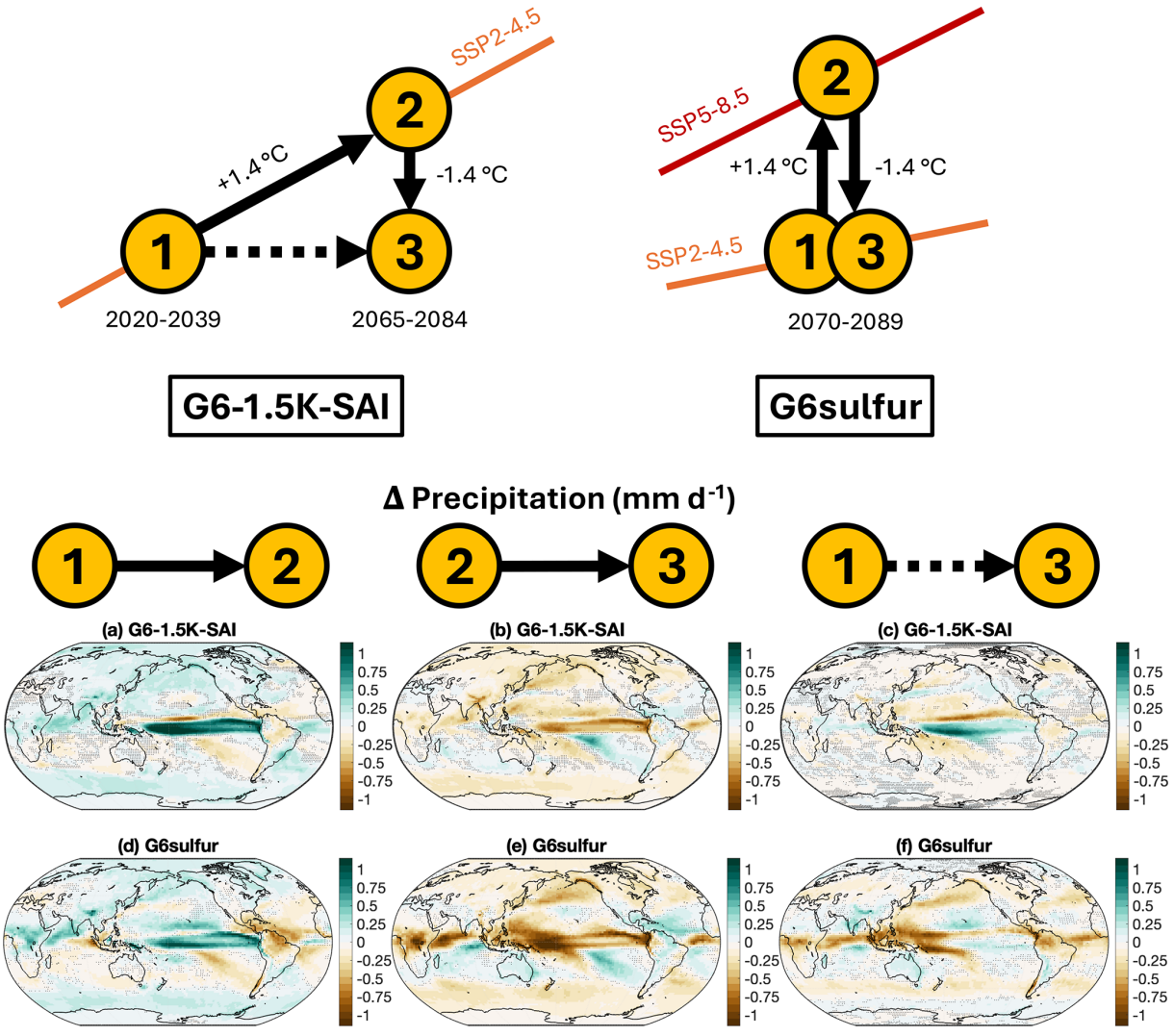

Figure 8. Multi-model mean maps of differences in precipitation (in mm d^{-1}) for G6-1.5K-SAI and G6sulfur and their respective warming scenarios, as in Fig. 6.

drying in the midlatitudes in both hemispheres is also more pronounced for G6sulfur than for G6-1.5K-SAI.

In the Supplementary Material (Sect. S3), we provide additional diagnostics characterizing the intertropical convergence zone (ITCZ). The impacts of SAI on the ITCZ are frequently cited as an important metric; it is known that preferentially forcing one hemisphere would be expected to shift the ITCZ towards the opposite hemisphere (e.g., Haywood et al., 2013), and the choice to manage T_1 by Kravitz et al. (2016) was motivated by the goal of limiting disruption to tropical precipitation. Here, we compute the location of the ITCZ as the centroid of zonal mean tropical precipitation between 20° N and 20° S latitude (e.g., Lee et al., 2020, after Donohoe et al., 2013; Frierson and Hwang, 2012); we also compute the strength of the ITCZ as the maximum zonal mean rainfall (Byrne et al., 2018) and the width of the ITCZ as the size of the latitude band containing the zonal maximum where precipitation exceeds 5 mm d^{-1} (after Wodzicki and Rapp, 2016). While we refrain from a detailed analysis, changes in ITCZ location for G6sulfur and G6-1.5K-SAI models are small relative to variability, and increases in ITCZ strength and width under global warming tend to be mitigated under G6-1.5K-SAI and mitigated or overcompensated by G6sulfur.

In Fig. 9, we present a comparison of hydrological sensitivity for G6-1.5K-SAI and G6sulfur. It is commonly seen in SRM simulations that cooling the entire planet reduces precipitation by a greater extent than it increased under the amount of warming to be offset. In the G1 experiment (uniform solar dimming to offset the forcing increase from an abrupt quadrupling of CO_2 concentrations), precipitation decreased by 2 %–6 % relative to preindustrial control in both CMIP5 and CMIP6 models (Tilmes et al., 2013; Kravitz et al., 2021); in SAI simulations, precipitation decreases rela-

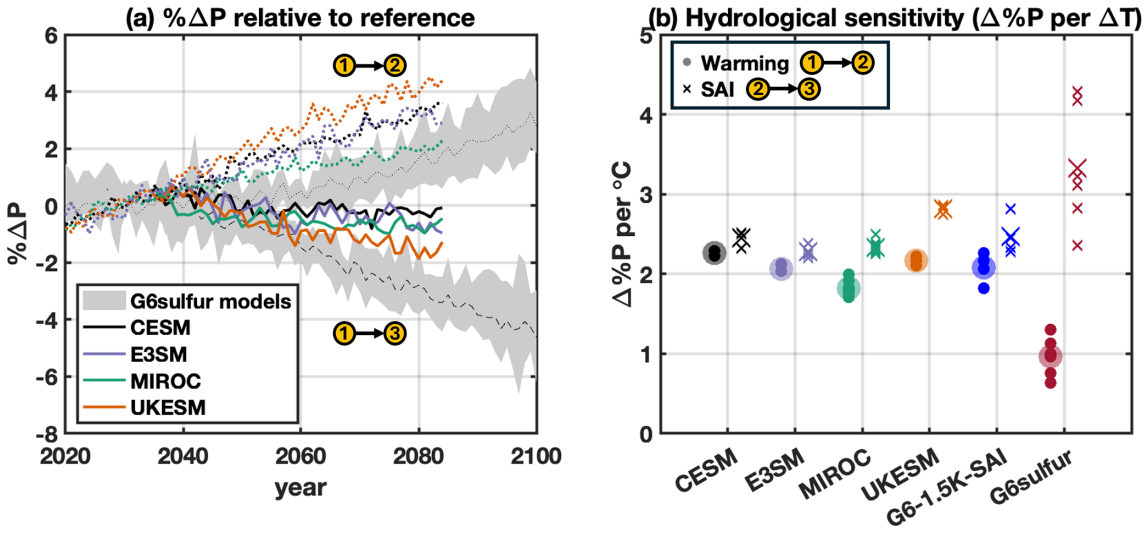

Figure 9. Precipitation (P) changes and hydrological sensitivity for G6-1.5K-SAI- and G6sulfur-participating models. Panel **(a)** plots changes in global mean precipitation over time, expressed as a % change relative to each model's reference (the SSP2-4.5 2020–2039 mean for G6-1.5K-SAI models, and SSP2-4.5 for G6sulfur models). Colored lines represent ensemble means of G6-1.5K-SAI-participating models, and gray shading denotes the spread of ensemble means of G6sulfur-participating models; dotted lines (values > 0) are for warming scenarios (SSP2-4.5 for G6-1.5K-SAI, and SSP5-8.5 for G6sulfur) and solid/dashed lines (values < 0) are for intervention scenarios (G6-1.5K-SAI and G6sulfur). Panel **(b)** plots hydrological sensitivity, defined as the % change in global mean precipitation (relative to the reference period) per degree of global mean temperature (T) change; for both panels, periods 1, 2, and 3 are defined as in Figs. 5–8. Dots indicate warming scenarios (% increase in P per °C of global warming), and x's indicate SAI scenarios (% decrease in P per °C of global warming). For individual G6-1.5K-SAI participating models (left four columns), small symbols denote individual ensemble members, and large symbols denote ensemble means; for multi-model means (right two columns), small symbols denote ensemble means of individual models, and large symbols denote multi-model means (models weighted equally).

tive to the reference in GLENS (Kravitz et al., 2017), ARISE-SAI-1.5 in both models (Richter et al., 2022; Henry et al., 2023), UKESM1's G6controller (Wells et al., 2024), and G6sulfur in all participating models (Fig. 9); and there is residual warming in a CESM2 SAI experiment controlling for global mean precipitation (Lee et al., 2020). In the G6-1.5K-SAI simulations, global mean precipitation also decreases relative to that of the reference period (SSP2-4.5 2020–2039) in all participating models.

The residual decrease in precipitation for G6-1.5K-SAI is smaller than for G6sulfur; this result is a combination of both the difference in scenario (larger precipitation increases in the warming scenario of G6-1.5K-SAI) and differences in the effects of the intervention (smaller absolute decreases in precipitation for G6-1.5K-SAI). Between 2020–2039 and 2065–2084 in the SSP2-4.5 scenario for G6-1.5K-SAI-participating models, precipitation increases by $0.09 \pm 0.03\,\mathrm{mm\,d^{-1}}$; in G6sulfur-participating models, in SSP5-8.5 2070–2089, relative to SSP2-4.5 2070–2089, precipitation increases by only $0.05 \pm 0.02\,\mathrm{mm\,d^{-1}}$. G6-1.5K-SAI models, on average, reduce precipitation by $0.11 \pm 0.04\,\mathrm{mm\,d^{-1}}$ during the 2065–2084 period, when they cool the planet by $\sim 1.4\,°\mathrm{C}$; during the period when G6sulfur models cool the planet by $\sim 1.4\,°\mathrm{C}$ (2070–2089), they reduce precipitation by $0.14 \pm 0.03\,\mathrm{mm\,d^{-1}}$. Differences in hydrological sensitivity between G6sulfur and G6-1.5K-SAI could be due to the difference in scenario as well as the difference in strategy; Duffey and Irvine (2024) analyzed a similar pair of experiments (G6sulfur and ARISE-SAI-1.5) and suggest that the choice of stabilized vs. transient temperature target can also affect hydrological response to SAI.

4 Discussion and Conclusions

In this manuscript, we present and discuss the initial results of the G6-1.5K-SAI experiment, in which four Earth system models simulate SAI under the SSP2-4.5 greenhouse gas emission pathway to maintain global mean surface temperatures at the levels corresponding to the 2020–2039 mean of the SSP2-4.5 simulation without SAI. The models show a range of background climate states and rates of warming, and require different rates of SO_2 injection and aerosol optical depth (AOD) to maintain their respective target temperatures. The models strongly agree on the cooling per rate of unit SO_2 injection ($0.11 \pm 0.01\,°\mathrm{C\,(Tg\,SO_2\,yr^{-1})^{-1}}$); this value is similar to that seen in G6sulfur models with interactive SO_2, and it also falls within the 8–16 $\mathrm{Tg\,SO_2\,yr^{-1}}$ per 1 °C range commonly cited in the literature (Haywood et al., 2022). However, the strong model agreement in this study may not imply accuracy due to similarities in aerosol rep-

resentation across models and disagreements between AOD per rate of unit injection and cooling per unit AOD which effectively cancel each other out. All four of the G6-1.5K-SAI-participating models use modal aerosol representation (see Table 2); additionally, CESM and E3SM both use versions of the same code (MAM) to represent aerosols. The 1991 eruption of Mt. Pinatubo is commonly cited as both motivation and validation for aerosol model performance: Gettelman et al. (2019), Mills et al. (2016) and Mills et al. (2017) describe the behavior of MAM in replicating the Pinatubo eruption, and/or changes made to the code to better replicate Pinatubo, at length; (Hu et al., 2025) introduces the 5th mode to MAM5 (used in E3SM) explicitly to better replicate Pinatubo; and CHASER/SPRINTARS (MIROC) and GLOMAP (UKESM) have also been used to study Pinatubo in depth, and have been shown to replicate well the observed global stratospheric aerosol optical depth following the eruption (see Sekiya et al., 2016; Dhomse et al., 2014, respectively). While it is of course not a bad thing that models train on volcanic eruptions, or that they can reproduce them well, there is no real-life observational analogue to the magnitude and duration of SAI considered in this study. It is plausible that models with similar aerosol representation and similar training and validation data could converge to a similar answer (i.e., for cooling per unit injection, as seen in Fig. 2c) that is not the ground truth. Running the G6-1.5K-SAI experiment in models that use other aerosol treatments, such as a less-complex bulk treatment or more-complex sectional treatment, could help better bound and explore such uncertainties.

Additionally, the G6-1.5K-SAI models demonstrate smaller nonlinearities in AOD with increasing injection rates than the G6sulfur models. Past model studies that examined these nonlinearities for very large injection rates (Niemeier and Timmreck, 2015; Niemeier and Tilmes, 2017) have found that AOD per rate of unit injection is fairly linear until rates of 10–20 $\mathrm{Tg\,SO_2\,yr^{-1}}$; however, G6sulfur models show decreasing AOD even early in the experiment, and most of the G6-1.5K-SAI models (excepting CESM) show small or nonexistent nonlinearities even as injection rates increase above 10 $\mathrm{Tg\,SO_2\,yr^{-1}}$. The G6-1.5K-SAI models report injected sulfur lifetime ranging from approximately 8 to 17 months and peak aerosol effective radius ranging from approximately 0.3 to 0.45 µm in the lower stratosphere.

The models also agree on several characteristics in the pattern of surface responses to both the SSP2-4.5 warming scenario and the G6-1.5K-SAI intervention. All four models demonstrate Arctic amplification and the land surface warming more quickly than the ocean surface, resulting in a net warming of the NH relative to the SH; G6-1.5K-SAI mitigates all of these patterns, but to what extents relative to SSP2-4.5 is model-dependent. SSP2-4.5 increases mid- and high-latitude annual mean precipitation, and G6-1.5K-SAI decreases it by comparable magnitudes in all four models. Changes to tropical precipitation in both scenarios are more complex, and models do not fully agree on the pattern of change. In comparing periods where G6-1.5K-SAI and G6sulfur cool the planet by approximately 1.4 °C, G6-1.5K-SAI cools the Arctic more effectively than G6sulfur, and decreases to precipitation (especially in the tropics and over land) are smaller for G6-1.5K-SAI than for G6sulfur. However, differences in the impacts of these strategies are representative of both differences in intervention strategy and differences in warming scenario, and therefore must be evaluated carefully.

The G6-1.5K-SAI experiment, like past GeoMIP experiments, can help identify, quantify, and bound uncertainties in the planetary response to SAI; in this study, we have discussed relationships between SO_2 injection rates, AOD, and global cooling; aerosol size and lifetime; and surface temperature and precipitation response, and how many of these impacts, relationships, and uncertainties have changed relative to G6sulfur. However, such an experiment cannot fully address all uncertainties. Eastham et al. (2025, Sect. 2.1 and Appendix B) discuss gaps in aerosol representation in SAI modeling, including microphysics and size distribution, radiation and chemistry interactions, and plume dynamics; sulfate aerosol representation is often validated against, for example, the 1991 Pinatubo eruption, but the dynamics and microphysics of a single-source point injection would differ from those of a continuous replenishment of the aerosol layer via, for example, fleets of aircraft (e.g. Smith, 2020). Eastham, et al. recommend that small laboratory and outdoor experiments would be the best path to resolving such uncertainties.

The G6-1.5K-SAI injection strategy – hemispherically symmetric injection at 30° latitude – was chosen to balance simplicity and optimality for a multi-model comparison. In this experiment, only the total amount of SO_2 injection is managed, and only GMSAT is regulated; in managing surface temperature alone, at least two more major degrees of freedom have been identified (interhemispheric and equator-to-pole temperature gradients, commonly called T_1 and T_2) which can be regulated independently with injections at additional latitudes. Therefore, we do not claim that 30° N + 30° S injection is the optimal strategy for any model. Additionally, 2020–2039 temperatures (in any model) is not necessarily the ideal climate, but rather a reference to measure the impacts of SAI relative to the impacts of global warming. However, the individual model responses here can provide insight into how surface temperatures might be further modulated by modifying the injection strategy. For example, G6-1.5K-SAI in CESM2 overcools the NH and undercools the SH, suggesting that more SH injection would provide a more even cooling of the planet, a result consistent with the ARISE-SAI-1.5 experiment. In contrast, UKESM1.1 has substantial residual Arctic warming, which injection closer to the pole could offset; this is similar to what was seen in the previous model version, as ARISE-SAI-1.5 and G6controller found that 30° injection in UKESM1 was

insufficiently poleward to fully manage T_2 (i.e., minimize changes in polar temperatures) in those experiments. We can also infer potential trade-offs between injection strategies; for instance, MIROC, like UKESM1.1, has several degrees of residual Arctic warming under G6-1.5K-SAI, but also has relatively little statistically significant change to annual mean precipitation compared to the baseline. While higher injection latitude(s) may mitigate Arctic amplification more effectively, changing the injection strategy could also plausibly reduce the effectiveness of SAI at maintaining baseline precipitation in MIROC. As such, future multi-model comparisons with different strategies and objectives would provide further valuable insights into SAI impacts, efficiencies and trade-offs, and thus inform both modeling community and policy.

Data availability. Data used in this study for G6-1.5K-SAI-participating models has been archived via the Zenodo online repository at https://doi.org/10.5281/zenodo.17613419 (Lee, 2025). Data used in this study from the G6sulfur experiment is available online through the Earth System Grid at https://esgf-node.llnl.gov/search/cmip6/ (WCRP, 2019).

Supplement. The supplement related to this article is available online at https://doi.org/10.5194/acp-26-7463-2026-supplement.

Author contributions. WRL drafted the manuscript, with review and assistance from all coauthors. WRL (CESM), BW and CW (E3SM), SW and TS (MIROC), and AJ, JH, and MH (UKESM) ran model simulations. DV and WRL provided guidance to modeling teams.

Competing interests. At least one of the (co-)authors is a member of the editorial board of *Atmospheric Chemistry and Physics*. The peer-review process was guided by an independent editor, and the authors also have no other competing interests to declare.

Disclaimer. Publisher's note: Copernicus Publications remains neutral with regard to jurisdictional claims made in the text, published maps, institutional affiliations, or any other geographical representation in this paper. The authors bear the ultimate responsibility for providing appropriate place names. Views expressed in the text are those of the authors and do not necessarily reflect the views of the publisher.

Acknowledgements. The authors would like to thank three anonymous reviewers, as well as Simone Tilmes (NSF NCAR), Kanishk Gohil (NSF NCAR), Douglas MacMartin (Cornell University), and Margot Clyne (University of Colorado Boulder), for comments and suggestions which contributed to the development of the paper.

Support for WRL has been provided by the Quadrature Climate Foundation. SW and TS are supported by the Environment Research and Technology Development Fund S-20 of the Environmental Restoration and Conservation Agency of Japan and the JSPS KAKENHI program. Support for MH, AJ, and JH was provided by SilverLining's Safe Climate Research Initiative (SCRI). JH also acknowledges support provided by Quadrature Climate Foundation. Support for BK was provided in part by NOAA's Climate Program Office, NOAA's Earth's Radiation Budget (ERB) program, and the Indiana University Environmental Resilience Institute. The Pacific Northwest National Laboratory is operated for the US Department of Energy by Battelle Memorial Institute under contract DE-AC05-76RL01830. EMB acknowledges support by the National Oceanic and Atmospheric Administration (NOAA), NOAA Earth Radiative Budget (ERB) program, and Reflective fellowship program.

The CESM project is supported primarily by the National Science Foundation. Computational support and computer and data storage services, including the Derecho supercomputer (NCAR, 2025), were provided by the Computational and Information Systems Laboratory (CISL) at NSF NCAR. Sandia National Laboratories is a multimission laboratory managed and operated by National Technology & Engineering Solutions of Sandia, LLC, a wholly owned subsidiary of Honeywell International Inc., for the U.S. Department of Energy's National Nuclear Security Administration under contract DE-NA0003525. This paper describes objective technical results and analysis. Any subjective views or opinions that might be expressed in the paper do not necessarily represent the views of the U.S. Department of Energy or the United States Government. The MIROC-ES2H was developed under the support of MEXT-Program for the advanced studies of climate change projection (SENTAN) Grant Number JPMXD0722681344 and simulations were conducted using the Earth Simulator at the JAMSTEC.

Financial support. This research has been supported by the Quadrature Climate Foundation (grant no. 01-21-000349), the Japan Society for the Promotion of Science (grant no. JP25K03324), the National Oceanic and Atmospheric Administration (grant nos. NA22OAR4310479 and NA22OAR4320151), and the Environment Research and Technology Development Fund S-20 of the Environmental Restoration and Conservation Agency of Japan, grant number JPMEERF21S12010.

Review statement. This paper was edited by Matthew Toohey and reviewed by three anonymous referees.

References

Baur, S., Sanderson, B. M., Séférian, R., and Terray, L.: Change in Wind Renewable Energy Potential Under Stratospheric Aerosol Injections, Earth's Future, 12, https://doi.org/10.1029/2024EF004575, 2024.

Bednarz, E. M., Butler, A. H., Visioni, D., Zhang, Y., Kravitz, B., and MacMartin, D. G.: Injection strategy – a driver of atmospheric circulation and ozone response to stratospheric aerosol geoengineering, Atmos. Chem. Phys., 23, 13665–13684, https://doi.org/10.5194/acp-23-13665-2023, 2023.

Bednarz, E. M., Goddard, P. B., MacMartin, D. G., Visioni, D., Bailey, D., and Danabasoglu, G.: Stratospheric Aerosol Injection Could Prevent Future Atlantic Meridional Overturning Circulation Decline, But Injection Location is Key, Earth's Future, 13, https://doi.org/10.1029/2025EF005919, 2025.

Brown, H. Y., Wagman, B., Bull, D., Peterson, K., Hillman, B., Liu, X., Ke, Z., and Lin, L.: Validating a microphysical prognostic stratospheric aerosol implementation in E3SMv2 using observations after the Mount Pinatubo eruption, Geosci. Model Dev., 17, 5087–5121, https://doi.org/10.5194/gmd-17-5087-2024, 2024.

Budyko, M. I.: Climatic Changes, American Geophysical Union, https://doi.org/10.1029/SP010, 1977.

Burgess, M. G., Ritchie, J., Shapland, J., and Pielke, R.: IPCC baseline scenarios have over-projected CO_2 emissions and economic growth, Environ. Res. Lett., 16, 014016, https://doi.org/10.1088/1748-9326/abcdd2, 2020.

Byrne, M. P., Pendergrass, A. G., Rapp, A. D., and Wodzicki, K. R.: Response of the Intertropical Convergence Zone to Climate Change: Location, Width, and Strength, Current Climate Change Reports, 4, 355–370, https://doi.org/10.1007/s40641-018-0110-5, 2018.

Crutzen, P. J.: Albedo Enhancement by Stratospheric Sulfur Injections: A Contribution to Resolve a Policy Dilemma?, Climatic Change, 77, 211, https://doi.org/10.1007/s10584-006-9101-y, 2006.

Danabasoglu, G., Lamarque, J.-F., Bacmeister, J., Bailey, D. A., DuVivier, A. K., Edwards, J., Emmons, L. K., Fasullo, J., Garcia, R., Gettelman, A., Hannay, C., Holland, M. M., Large, W. G., Lauritzen, P. H., Lawrence, D. M., Lenaerts, J. T. M., Lindsay, K., Lipscomb, W. H., Mills, M. J., Neale, R., Oleson, K. W., Otto-Bliesner, B., Phillips, A. S., Sacks, W., Tilmes, S., van Kampenhout, L., Vertenstein, M., Bertini, A., Dennis, J., Deser, C., Fischer, C., Fox-Kemper, B., Kay, J. E., Kinnison, D., Kushner, P. J., Larson, V. E., Long, M. C., Mickelson, S., Moore, J. K., Nienhouse, E., Polvani, L., Rasch, P. J., and Strand, W. G.: The Community Earth System Model Version 2 (CESM2), J. Adv. Model. Earth Sy., 12, e2019MS001916, https://doi.org/10.1029/2019MS001916, 2020.

Dhomse, S. S., Emmerson, K. M., Mann, G. W., Bellouin, N., Carslaw, K. S., Chipperfield, M. P., Hommel, R., Abraham, N. L., Telford, P., Braesicke, P., Dalvi, M., Johnson, C. E., O'Connor, F., Morgenstern, O., Pyle, J. A., Deshler, T., Zawodny, J. M., and Thomason, L. W.: Aerosol microphysics simulations of the Mt. Pinatubo eruption with the UM-UKCA composition-climate model, Atmos. Chem. Phys., 14, 11221–11246, https://doi.org/10.5194/acp-14-11221-2014, 2014.

Donohoe, A., Marshall, J., Ferreira, D., and Mcgee, D.: The Relationship between ITCZ Location and Cross-Equatorial Atmospheric Heat Transport: From the Seasonal Cycle to the Last Glacial Maximum, J. Climate, 26, 3597–3618, https://doi.org/10.1175/JCLI-D-12-00467.1, 2013.

Duan, L., Cao, L., Bala, G., and Caldeira, K.: Climate Response to Pulse Versus Sustained Stratospheric Aerosol Forcing, Geophys. Res. Lett., 46, 8976–8984, https://doi.org/10.1029/2019GL083701, 2019.

Duffey, A. and Irvine, P. J.: Accounting for transience in the baseline climate state changes the surface climate response attributed to stratospheric aerosol injection, Environmental Research: Climate, 3, 041008, https://doi.org/10.1088/2752-5295/ad9f91, 2024.

Dykema, J. A., Keith, D. W., and Keutsch, F. N.: Improved aerosol radiative properties as a foundation for solar geoengineering risk assessment, Geophys. Res. Lett., 43, 7758–7766, https://doi.org/10.1002/2016GL069258, 2016.

Eastham, S. D., Butler, A. H., Doherty, S. J., Gasparini, B., Tilmes, S., Bednarz, E. M., Burkhardt, U., Chiodo, G., Cziczo, D. J., Diamond, M. S., Keith, D. W., Leisner, T., MacMartin, D. G., Quaas, J., Rasch, P. J., Sourdeval, O., Steinke, I., Thompson, C., Visioni, D., Wood, R., Xia, L., and Yu, P.: Key Gaps in Models' Physical Representation of Climate Intervention and Its Impacts, J. Adv. Model. Earth Sy., 17, https://doi.org/10.1029/2024MS004872, 2025.

Fernández, A., Manquehual-Cheuque, F., and Somos-Valenzuela, M.:, Impact of Solar Radiation Management on Andean glacier-wide surface mass balance, npj Climate and Atmospheric Science, 7, https://doi.org/10.1038/s41612-024-00807-x, 2024.

Fotso-Nguemo, T. C., Chouto, S., Nghonda, J. P., Diedhiou, A., Kravitz, B., Yepdo, Z. D., Djuidje, F. K., and Abiodun, B. J.: Projected impact of solar radiation modification geoengineering on water deficit risk over major Central African river basins, Environ. Res. Lett., 19, https://doi.org/10.1088/1748-9326/ad657d, 2024.

Frierson, D. M. W. and Hwang, Y.-T.: Extratropical Influence on ITCZ Shifts in Slab Ocean Simulations of Global Warming, J. Climate, 25, 720–733, https://doi.org/10.1175/JCLI-D-11-00116.1, 2012.

Gabriel, C. J. and Robock, A.: Stratospheric geoengineering impacts on El Niño/Southern Oscillation, Atmos. Chem. Phys., 15, 11949–11966, https://doi.org/10.5194/acp-15-11949-2015, 2015.

Gettelman, A., Mills, M. J., Kinnison, D. E., Garcia, R. R., Smith, A. K., Marsh, D. R., Tilmes, S., Vitt, F., Bardeen, C. G., McInerny, J., Liu, H.-L., Solomon, S. C., Polvani, L. M., Emmons, L. K., Lamarque, J.-F., Richter, J. H., Glanville, A. S., Bacmeister, J. T., Phillips, A. S., Neale, R. B., Simpson, I. R., DuVivier, A. K., Hodzic, A., and Randel, W. J.: The Whole Atmosphere Community Climate Model Version 6 (WACCM6), J. Geophys. Res.-Atmos., 124, 12380–12403, https://doi.org/10.1029/2019JD030943, 2019.

Grainger, R.: Some Useful Formulae for Particle Size Distributions and Optical Properties, https://eodg.atm.ox.ac.uk/user/grainger/research/aerosols.pdf (last access: 21 April 2026), 2025.

Haywood, J., Tilmes, S., Keutsch, F., Niemeier, U., Schmidt, A., Visioni, D., Yu, P., Dykema, J., Jones, A. C., Laasko, A., and Wilka, C. A.: Stratospheric Aerosol Injection and its Potential Effect on the Stratospheric Ozone Layer, in: Scientific Assessment of Ozone Depletion: 2022, edited by: Aquila, V. and Rosenlof, K. H., chap. 6, WMO, https://csl.noaa.gov/assessments/ozone/2022/downloads/Chapter6_2022OzoneAssessment.pdf (last access: 20 May 2026), 2022.

Haywood, J. M., Jones, A., Bellouin, N., and Stephenson, D.: Asymmetric forcing from stratospheric aerosols impacts Sahelian rainfall, Nat. Clim. Change, 3, 660–665, https://doi.org/10.1038/nclimate1857, https://doi.org/10.1038/nclimate1857, 2013.

Haywood, J. M., Boucher, O., Lennard, C., Storelvmo, T., Tilmes, S., and Visioni, D.: World Climate Research Programme light-

house activity: an assessment of major research gaps in solar radiation modification research, Frontiers in Climate, 7, https://doi.org/10.3389/fclim.2025.1507479, 2025.

Henry, M., Haywood, J., Jones, A., Dalvi, M., Wells, A., Visioni, D., Bednarz, E. M., MacMartin, D. G., Lee, W., and Tye, M. R.: Comparison of UKESM1 and CESM2 simulations using the same multi-target stratospheric aerosol injection strategy, Atmos. Chem. Phys., 23, 13369–13385, https://doi.org/10.5194/acp-23-13369-2023, 2023.

Henry, M., Bednarz, E. M., and Haywood, J.: How does the latitude of stratospheric aerosol injection affect the climate in UKESM1?, Atmos. Chem. Phys., 24, 13253–13268, https://doi.org/10.5194/acp-24-13253-2024, 2024.

Hu, A., Ke, Z., Liu, X., Wagman, B., Brown, H., Lu, Z., Wu, M., Wang, H., Tang, Q., Bull, D., Peterson, K., and Xie, S.: Size-resolved process understanding of stratospheric sulfate aerosol following the Pinatubo eruption, Atmos. Chem. Phys., 25, 12137–12157, https://doi.org/10.5194/acp-25-12137-2025, 2025.

Joshi, M. M., Gregory, J. M., Webb, M. J., Sexton, D. M. H., and Johns, T. C.: Mechanisms for the land/sea warming contrast exhibited by simulations of climate change, Clim. Dynam., 30, 455–465, https://doi.org/10.1007/s00382-007-0306-1, 2008.

Kawamiya, M., Hajima, T., Tachiiri, K., Watanabe, S., and Yokohata, T.: Two decades of Earth system modeling with an emphasis on Model for Interdisciplinary Research on Climate (MIROC), Progress in Earth and Planetary Science, 7, https://doi.org/10.1186/s40645-020-00369-5, 2020.

Kleinschmitt, C., Boucher, O., and Platt, U.: Sensitivity of the radiative forcing by stratospheric sulfur geoengineering to the amount and strategy of the SO_2injection studied with the LMDZ-S3A model, Atmos. Chem. Phys., 18, 2769–2786, https://doi.org/10.5194/acp-18-2769-2018, 2018.

Kravitz, B., Robock, A., Boucher, O., Schmidt, H., Taylor, K. E., Stenchikov, G., and Schulz, M.: The Geoengineering Model Intercomparison Project (GeoMIP), Atmos. Sci. Lett., 12, 162–167, https://doi.org/10.1002/asl.316, 2011.

Kravitz, B., Robock, A., Tilmes, S., Boucher, O., English, J. M., Irvine, P. J., Jones, A., Lawrence, M. G., MacCracken, M., Muri, H., Moore, J. C., Niemeier, U., Phipps, S. J., Sillmann, J., Storelvmo, T., Wang, H., and Watanabe, S.: The Geoengineering Model Intercomparison Project Phase 6 (GeoMIP6): simulation design and preliminary results, Geosci. Model Dev., 8, 3379–3392, https://doi.org/10.5194/gmd-8-3379-2015, 2015.

Kravitz, B., MacMartin, D. G., Wang, H., and Rasch, P. J.: Geoengineering as a design problem, Earth Syst. Dynam., 7, 469–497, https://doi.org/10.5194/esd-7-469-2016, 2016.

Kravitz, B., MacMartin, D. G., Mills, M. J., Richter, J. H., Tilmes, S., Lamarque, J.-F., Tribbia, J. J., and Vitt, F.: First Simulations of Designing Stratospheric Sulfate Aerosol Geoengineering to Meet Multiple Simultaneous Climate Objectives, J. Geophys. Res.-Atmos., 122, 12616–12634, https://doi.org/10.1002/2017JD026874, 2017.

Kravitz, B., MacMartin, D. G., Visioni, D., Boucher, O., Cole, J. N. S., Haywood, J., Jones, A., Lurton, T., Nabat, P., Niemeier, U., Robock, A., Séférian, R., and Tilmes, S.: Comparing different generations of idealized solar geoengineering simulations in the Geoengineering Model Intercomparison Project (GeoMIP), Atmos. Chem. Phys., 21, 4231–4247, https://doi.org/10.5194/acp-21-4231-2021, 2021.

Lee, W. R.: Data for "G6-1.5K-SAI and G6sulfur: changes in impacts and uncertainty depending on stratospheric aerosol injection strategy in the Geoengineering Model Intercomparison Project", version v1, Zenodo [data set], https://doi.org/10.5281/zenodo.17613419, 2025.

Lee, W., MacMartin, D., Visioni, D., and Kravitz, B.: Expanding the design space of stratospheric aerosol geoengineering to include precipitation-based objectives and explore trade-offs, Earth Syst. Dynam., 11, 1051–1072, https://doi.org/10.5194/esd-11-1051-2020, 2020.

Lee, W. R., Visioni, D., Bednarz, E. M., MacMartin, D. G., Kravitz, B., and Tilmes, S.: Quantifying the Efficiency of Stratospheric Aerosol Geoengineering at Different Altitudes, Geophys. Res. Lett., 50, e2023GL104417, https://doi.org/10.1029/2023GL104417, 2023.

Liu, X., Easter, R. C., Ghan, S. J., Zaveri, R., Rasch, P., Shi, X., Lamarque, J.-F., Gettelman, A., Morrison, H., Vitt, F., Conley, A., Park, S., Neale, R., Hannay, C., Ekman, A. M. L., Hess, P., Mahowald, N., Collins, W., Iacono, M. J., Bretherton, C. S., Flanner, M. G., and Mitchell, D.: Toward a minimal representation of aerosols in climate models: description and evaluation in the Community Atmosphere Model CAM5, Geosci. Model Dev., 5, 709–739, https://doi.org/10.5194/gmd-5-709-2012, 2012.

Liu, X., Ma, P.-L., Wang, H., Tilmes, S., Singh, B., Easter, R. C., Ghan, S. J., and Rasch, P. J.: Description and evaluation of a new four-mode version of the Modal Aerosol Module (MAM4) within version 5.3 of the Community Atmosphere Model, Geosci. Model Dev., 9, 505–522, https://doi.org/10.5194/gmd-9-505-2016, 2016.

MacMartin, D. G., Kravitz, B., Tilmes, S., Richter, J. H., Mills, M. J., Lamarque, J.-F., Tribbia, J. J., and Vitt, F.: The Climate Response to Stratospheric Aerosol Geoengineering Can Be Tailored Using Multiple Injection Locations, J. Geophys. Res.-Atmos., 122, 12574–12590, https://doi.org/10.1002/2017JD026868, 2017.

MacMartin, D. G., Visioni, D., Kravitz, B., Richter, J. H., Felgenhauer, T., Lee, W. R., Morrow, D. R., Parson, E. A., and Sugiyama, M.: Scenarios for modeling solar radiation modification, P. Natl. Acad. Sci. USA, https://doi.org/10.1073/pnas.2202230119, 2022.

Mayer, K. J., Barnes, E. A., and Hurrell, J. W.: Future seasonal surface temperature predictability with and without ARISE-stratospheric aerosol injection-1.5, Environmental Research: Climate, 3, 045026, https://doi.org/10.1088/2752-5295/ad9b43, 2024.

Mills, M. J., Schmidt, A., Easter, R., Solomon, S., Kinnison, D. E., Ghan, S. J., Neely III, R. R., Marsh, D. R., Conley, A., Bardeen, C. G., and Gettelman, A.: Global volcanic aerosol properties derived from emissions, 1990–2014, using CESM1(WACCM), J. Geophys. Res.-Atmos., 121, 2332–2348, https://doi.org/10.1002/2015JD024290, 2016.

Mills, M. J., Richter, J. H., Tilmes, S., Kravitz, B., MacMartin, D. G., Glanville, A. A., Tribbia, J. J., Lamarque, J.-F., Vitt, F., Schmidt, A., Gettelman, A., Hannay, C., Bacmeister, J. T., and Kinnison, D. E.: Radiative and Chemical Response to Interactive Stratospheric Sulfate Aerosols in Fully Cou-

pled CESM1(WACCM), J. Geophys. Res.-Atmos., 122, 13061–13078, https://doi.org/10.1002/2017JD027006, 2017.

Moore, J. C., Yue, C., Chen, Y., Jevrejeva, S., Visioni, D., Uotila, P., and Zhao, L.: Multi-Model Simulation of Solar Geoengineering Indicates Avoidable Destabilization of the West Antarctic Ice Sheet, Earth's Future, 12, https://doi.org/10.1029/2024EF004424, 2024.

Mulcahy, J. P., Johnson, C., Jones, C. G., Povey, A. C., Scott, C. E., Sellar, A., Turnock, S. T., Woodhouse, M. T., Abraham, N. L., Andrews, M. B., Bellouin, N., Browse, J., Carslaw, K. S., Dalvi, M., Folberth, G. A., Glover, M., Grosvenor, D. P., Hardacre, C., Hill, R., Johnson, B., Jones, A., Kipling, Z., Mann, G., Mollard, J., O'Connor, F. M., Palmiéri, J., Reddington, C., Rumbold, S. T., Richardson, M., Schutgens, N. A. J., Stier, P., Stringer, M., Tang, Y., Walton, J., Woodward, S., and Yool, A.: Description and evaluation of aerosol in UKESM1 and HadGEM3-GC3.1 CMIP6 historical simulations, Geosci. Model Dev., 13, 6383–6423, https://doi.org/10.5194/gmd-13-6383-2020, 2020.

Mulcahy, J. P., Jones, C. G., Rumbold, S. T., Kuhlbrodt, T., Dittus, A. J., Blockley, E. W., Yool, A., Walton, J., Hardacre, C., Andrews, T., Bodas-Salcedo, A., Stringer, M., de Mora, L., Harris, P., Hill, R., Kelley, D., Robertson, E., and Tang, Y.: UKESM1.1: development and evaluation of an updated configuration of the UK Earth System Model, Geosci. Model Dev., 16, 1569–1600, https://doi.org/10.5194/gmd-16-1569-2023, 2023.

National Academies of Sciences, Engineering, and Medicine: Reflecting Sunlight: Recommendations for Solar Geoengineering Research and Research Governance, The National Academies Press, Washington, DC, ISBN 978-0-309-67605-2, https://doi.org/10.17226/25762, 2021.

NCAR: User Documentation for NSF NCAR High Performance Computing, https://doi.org/10.5065/qx9a-pg09, 2025.

Niemeier, U. and Tilmes, S.: Sulfur injections for a cooler planet, Science, 357, 246–248, https://doi.org/10.1126/science.aan3317, 2017.

Niemeier, U. and Timmreck, C.: What is the limit of climate engineering by stratospheric injection of SO_2?, Atmos. Chem. Phys., 15, 9129–9141, https://doi.org/10.5194/acp-15-9129-2015, 2015.

O'Neill, B. C., Kriegler, E., Riahi, K., Ebi, K. L., Hallegatte, S., Carter, T. R., Mathur, R., and van Vuuren, D. P.: A new scenario framework for climate change research: the concept of shared socioeconomic pathways, Climatic Change, 122, 387–400, https://doi.org/10.1007/s10584-013-0905-2, 2014.

O'Neill, B. C., Tebaldi, C., van Vuuren, D. P., Eyring, V., Friedlingstein, P., Hurtt, G., Knutti, R., Kriegler, E., Lamarque, J.-F., Lowe, J., Meehl, G. A., Moss, R., Riahi, K., and Sanderson, B. M.: The Scenario Model Intercomparison Project (ScenarioMIP) for CMIP6, Geosci. Model Dev., 9, 3461–3482, https://doi.org/10.5194/gmd-9-3461-2016, 2016.

Rezaei, A., Karami, K., Tilmes, S., and Moore, J. C.: Changes in global teleconnection patterns under global warming and stratospheric aerosol intervention scenarios, Atmos. Chem. Phys., 23, 5835–5850, https://doi.org/10.5194/acp-23-5835-2023, 2023.

Richter, J. H., Visioni, D., MacMartin, D. G., Bailey, D. A., Rosenbloom, N., Dobbins, B., Lee, W. R., Tye, M., and Lamarque, J.-F.: Assessing Responses and Impacts of Solar climate intervention on the Earth system with stratospheric aerosol injection (ARISE-SAI): protocol and initial results from the first simulations, Geosci. Model Dev., 15, 8221–8243, https://doi.org/10.5194/gmd-15-8221-2022, 2022.

Sekiya, T., Sudo, K., and Nagai, T.: Evolution of stratospheric sulfate aerosol from the 1991 Pinatubo eruption: Roles of aerosol microphysical processes, J. Geophys. Res.-Atmos., 121, 2911–2938, https://doi.org/10.1002/2015JD024313, 2016.

Shine, K., Beerling, D., Carslaw, K., Haywood, J., Henry, M., Irvine, P., Maycock, A., Palmer, T., Rowan, S., Schmidt, A., and Wilcox, L.: Solar radiation modification policy briefing, The Royal Society, https://royalsociety.org/-/media/policy/projects/solar-radiation-modification/solar-radiation-modification-policy-briefing.pdf (last access: 20 May 2026), 2025.

Smith, W.: The cost of stratospheric aerosol injection through 2100, Environ. Res. Lett., 15, https://doi.org/10.1088/1748-9326/aba7e7, 2020.

Sutton, R. T., Dong, B., and Gregory, J. M.: Land/sea warming ratio in response to climate change: IPCC AR4 model results and comparison with observations, Geophys. Res. Lett., 34, https://doi.org/10.1029/2006GL028164, 2007.

Taylor, P. C., Boeke, R. C., Boisvert, L. N., Feldl, N., Henry, M., Huang, Y., Langen, P. L., Liu, W., Pithan, F., Sejas, S. A., and Tan, I.: Process Drivers, Inter-Model Spread, and the Path Forward: A Review of Amplified Arctic Warming, Frontiers in Earth Science, 9, https://doi.org/10.3389/feart.2021.758361, 2022.

Tilmes, S., Fasullo, J., Lamarque, J.-F., Marsh, D. R., Mills, M., Alterskjær, K., Muri, H., Kristjánsson, J. E., Boucher, O., Schulz, M., Cole, J. N. S., Curry, C. L., Jones, A., Haywood, J., Irvine, P. J., Ji, D., Moore, J. C., Karam, D. B., Kravitz, B., Rasch, P. J., Singh, B., Yoon, J.-H., Niemeier, U., Schmidt, H., Robock, A., Yang, S., and Watanabe, S.: The hydrological impact of geoengineering in the Geoengineering Model Intercomparison Project (GeoMIP), J. Geophys. Res.-Atmos., 118, 11036–11058, https://doi.org/10.1002/jgrd.50868, 2013.

Tilmes, S., Richter, J. H., Kravitz, B., MacMartin, D. G., Mills, M. J., Simpson, I. R., Glanville, A. S., Fasullo, J. T., Phillips, A. S., Lamarque, J.-F., Tribbia, J., Edwards, J., Mickelson, S., and Ghosh, S.: CESM1(WACCM) Stratospheric Aerosol Geoengineering Large Ensemble Project, B. Am. Meteorol. Soc., 99, 2361–2371, https://doi.org/10.1175/BAMS-D-17-0267.1, 2018.

Tilmes, S., MacMartin, D. G., Lenaerts, J. T. M., van Kampenhout, L., Muntjewerf, L., Xia, L., Harrison, C. S., Krumhardt, K. M., Mills, M. J., Kravitz, B., and Robock, A.: Reaching 1.5 and 2.0 °C global surface temperature targets using stratospheric aerosol geoengineering, Earth Syst. Dynam., 11, 579–601, https://doi.org/10.5194/esd-11-579-2020, 2020.

Visioni, D., Pitari, G., Tuccella, P., and Curci, G.: Sulfur deposition changes under sulfate geoengineering conditions: quasi-biennial oscillation effects on the transport and lifetime of stratospheric aerosols, Atmos. Chem. Phys., 18, 2787–2808, https://doi.org/10.5194/acp-18-2787-2018, 2018.

Visioni, D., MacMartin, D. G., Kravitz, B., Boucher, O., Jones, A., Lurton, T., Martine, M., Mills, M. J., Nabat, P., Niemeier, U., Séférian, R., and Tilmes, S.: Identifying the sources of uncertainty in climate model simulations of solar radiation modification with the G6sulfur and G6solar Geoengineering Model Intercomparison Project (GeoMIP) simulations, Atmos. Chem. Phys., 21, 10039–10063, https://doi.org/10.5194/acp-21-10039-2021, 2021.

Visioni, D., Bednarz, E. M., Lee, W. R., Kravitz, B., Jones, A., Haywood, J. M., and MacMartin, D. G.: Climate response to off-equatorial stratospheric sulfur injections in three Earth system models – Part 1: Experimental protocols and surface changes, Atmos. Chem. Phys., 23, 663–685, https://doi.org/10.5194/acp-23-663-2023, 2023.

Visioni, D., Robock, A., Haywood, J., Henry, M., Tilmes, S., MacMartin, D. G., Kravitz, B., Doherty, S. J., Moore, J., Lennard, C., Watanabe, S., Muri, H., Niemeier, U., Boucher, O., Syed, A., Egbebiyi, T. S., Séférian, R., and Quaglia, I.: G6-1.5K-SAI: a new Geoengineering Model Intercomparison Project (GeoMIP) experiment integrating recent advances in solar radiation modification studies, Geosci. Model Dev., 17, 2583–2596, https://doi.org/10.5194/gmd-17-2583-2024, 2024.

WCRP: CMIP6 project data, WCRP [data set], https://esgf-node.llnl.gov/search/cmip6/ (25 October 2025), 2019.

Wells, A. F., Henry, M., Bednarz, E. M., MacMartin, D. G., Jones, A., Dalvi, M., and Haywood, J. M.: Identifying Climate Impacts From Different Stratospheric Aerosol Injection Strategies in UKESM1, Earth's Future, 12, https://doi.org/10.1029/2023EF004358, 2024.

Wodzicki, K. R. and Rapp, A. D.: Long-term characterization of the Pacific ITCZ using TRMM, GPCP, and ERA-Interim, J. Geophys. Res.-Atmos., 121, 3153–3170, https://doi.org/10.1002/2015JD024458, 2016.

Xie, S., Terai, C. R., Wang, H., Tang, Q., Fan, J., Burrows, S. M., Lin, W., Wu, M., Song, X., Zhang, Y., Taylor, M. A., Golaz, J.-C., Benedict, J. J., Chen, C.-C., Feng, Y., Hannah, W. M., Ke, Z., Shan, Y., Larson, V. E., Liu, X., Prather, M. J., Richter, J. H., Shrivastava, M., Wan, H., Zhang, G. J., Zhang, K., Bradley, A., Cameron-Smith, P. J., Damiano, L., Debusschere, B., Donahue, A. S., Easter, R. C., Eldred, M. S., Griffin, B. M., Guba, O., Guo, Z., Huang, X., Lee, J., Lee, H.-H., Lou, S., Mahfouz, N., Moncrieff, M. W., Mülmenstädt, J., Qian, Y., Rasool, Q. Z., Roberts, A., Santos, S. P., Sargsyan, K., Shpund, J., Singh, B., Tao, C., Xie, J., Yang, Y., Zeng, X., Zhang, C., Zhang, M., Zhang, S., Zhang, T., Zheng, X., Jacob, R. L., Leung, L. R., McCoy, R., and Bader, D. C.: The Energy Exascale Earth System Model Version 3. Part I: Overview of the Atmospheric Component, ESS Open Archive [preprint], https://doi.org/10.22541/essoar.174456922.21825772/v1, 2025.

Zhang, Y., MacMartin, D. G., Visioni, D., Bednarz, E. M., and Kravitz, B.: Hemispherically symmetric strategies for stratospheric aerosol injection, Earth Syst. Dynam., 15, 191–213, https://doi.org/10.5194/esd-15-191-2024, 2024.